Accepted Manuscript

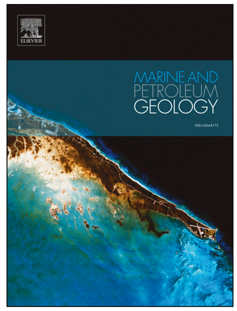

The prospectivity of a potential shale gas play: An example from the southern Pennine Basin (central England, UK)

Jan A.I. Hennissen, Edward Hough, Christopher H. Vane, Melanie J. Leng, Simon J. Kemp, Michael H. Stephenson

PII: S0264-8172(17)30240-4

DOI: 10.1016/j.marpetgeo.2017.06.033

Reference: JMPG 2967

To appear in: *Marine and Petroleum Geology*

Received Date: 23 March 2017

Revised Date: 19 June 2017

Accepted Date: 21 June 2017

Please cite this article as: Hennissen, J.A.I., Hough, E., Vane, C.H., Leng, M.J., Kemp, S.J., Stephenson, M.H., The prospectivity of a potential shale gas play: An example from the southern Pennine Basin (central England, UK), *Marine and Petroleum Geology* (2017), doi: 10.1016/j.marpetgeo.2017.06.033.

The prospectivity of a potential shale gas play: an example from the southern Pennine Basin (central England, UK)

Jan A. I. Hennissen[a*], Edward Hough[a], Christopher H. Vane[a], Melanie J. Leng[a,b,c], Simon J. Kemp[a] Michael H. Stephenson[a]

[a]*British Geological Survey, Environmental Science Centre, Nicker Hill, Keyworth, Nottingham, NG12 5GG, United Kingdom*

[b]*NERC Isotope Geosciences Facilities, British Geological Survey, Keyworth, Nottingham NG12 5GG, United Kingdom*

[c]*Centre for Environmental Geochemistry, University of Nottingham NG7 2DD, United Kingdom*

[*]Corresponding author. Tel: +44(0) 115 936 3532.

E-mail address: janh@bgs.ac.uk (J. Hennissen).

Abstract

During the Serpukhovian (late Mississippian) Stage, the Pennine Basin, now underlying much of northern England, consisted of a series of interlinked sub-basins that developed in response to the crustal extension north of the Hercynic orogenic zone. For the current study, mudstone samples of the Morridge Formation from two sub-basins located in the south-eastern part of the Pennine Basin were collected from the Carsington Dam Reconstruction C3 Borehole (Widmerpool Gulf sub-basin) and the Karenight 1 Borehole (Edale Gulf sub-basin). Detailed palynological analyses indicate that aside from the dominant (often 90% or more) heterogeneous amorphous organic matter (AOM), variable abundances of homogeneous AOM and phytoclasts are present. To complement the palynological dataset, a suite of geochemical and mineralogical techniques were applied to evaluate the prospectivity of these potentially important source rocks. Changes in the carbon isotope composition of the bulk organic fraction ($\delta^{13}C_{OM}$) suggest that the lower part (Biozone E_{2a}) of Carsington DR C3 is

markedly more influenced by terrigenous kerogen than the upper part of the core (Biozones E_{2a3}–E_{2b1}). The Karenight 1 core yielded more marine kerogen in the lower part (Marine Bands E_1–E_{2b}) than the upper part (Marine Band E_{2b}). Present day Rock-Eval™ Total Organic Carbon (TOC) surpasses 2% in most samples from both cores, a proportion suggested by Jarvie (2012) that defines prospective shale gas reservoirs. However, when the pyrolysable component that reflects the generative kerogen fraction is considered, very few samples reach this threshold. The kerogen typing permits for the first time the calculation of an original hydrogen index (HI_o) and original total organic carbon (TOC_o) for Carboniferous mudstones of the Pennine Basin. The most prospective part of Carsington DR C3 (marine bands E_{2b1}–E_{2a3}) has an average TOC_o of 3.2% and an average HI_o of 465 mg/g TOC_o. The most prospective part of Karenight 1 (242.80–251.89 m) is characterized by an average TOC_o of 9.3% and an average HI_o of 504 mg/g TOC_o. Lastly, X-ray diffraction (XRD) analysis confirms that the siliceous to argillaceous mudstones contain a highly variable carbonate content. The palynological, geochemical and mineralogical proxies combined indicate that marine sediments were continuously being deposited throughout the sampled intervals and were punctuated by episodic turbiditic events. The terrestrial material, originating from the Wales-Brabant High to the south of the Pennine Basin, was principally deposited in the Widmerpool Gulf, with much less terrigenous organic matter reaching the Edale Gulf. As a consequence, the prospective intervals are relatively thin, decimetre- to meter-scale, and further high resolution characterization of these intervals is required to understand variability in prospectivitiy over these limited intervals.

1. Introduction

Between 1872 and 1876 two boreholes drilled in Netherfield (East Sussex, UK) were found to not only contain thick gypsum deposits (Sub-Wealden Exploration Company, 1873) but also inflammable gases from ‘petroleum bearing strata’ (Willett, 1875 in Blackwell, 2013). These findings were the result of the Sub-Wealden Exploration, an academic effort to complete the knowledge of the range of Palaeozoic rocks underneath the Weald (Topley et al., 1872). For more than a century, very little research was directed towards further exploring the prospectivity of this energy resource. Then, following the start of shale gas exploration in the United States in 1982 (Steward, 2007), interest of the research community in the UK was reinvigorated with efforts focused on Carboniferous organic-rich shales (Selley, 1987; Smith et al., 2010). More recently, the Namurian (Visean–Serpukhovian) Bowland Shale Formation and its lateral equivalents including the Edale Shale and the Morridge formations (Waters et al., 2007), were identified as the most promising targets (Andrews, 2013; Selley, 2012; Smith et al., 2010). These British Namurian-aged shales were deposited in a mosaic of interlinked basins in a proximal position with emergent areas to the north (the Southern Uplands) and the south (Wales Brabant High) serving as the main sources of terrigenous material (Figures 1, 2) (Aitkenhead et al., 2002; Fraser and Gawthorpe, 1990; Waters et al., 2009). During the Mississippian (359–323.2 Ma), the Pennine Basin was located in an equatorial position, proximal to Laurussia with Gondwana stretching to the South Pole (McKerrow and Scotese, 1990), bordered by two emerging land masses. Because of its position, ice sheets were likely to persist on Gondwana (Isbell et al., 2003) which influenced the sedimentation history in the patchwork of sub-basins forming the Pennine Basin (e.g. Stephenson et al., 2010).

Here we present a high resolution, multiproxy dataset to characterize the potentially prospective intervals of the Mississippian successions in the southern part of the Pennine Basin. We present geochemical (Rock-Eval^{TM}, organic carbon isotopes), palynological and lithological-mineralogical (X-ray diffraction, XRD) results from two cored boreholes: Carsington Reconstruction Borehole C3 (British Geological Survey reference number SK25SW/113) and Karenight 1 (British Geological Survey reference number SK36NW/13). The former was drilled in the Widmerpool Gulf while the latter originates close to the Derbyshire High–Edale Gulf boundary (Figures 1, 2). In both boreholes we studied an interval containing the E_{2a} marine band, which is part of the late Serpukhovian (late Mississippian). This interval was chosen because of the availability of pre-existing data (e.g. Könitzer, 2014) on this marine band in the Widmerpool Gulf. The Karenight 1 core is one of very few well-preserved cores to prove the same interval from the Edale Gulf, a neighbouring sub-basin of the Widmerpool Gulf in the Pennine Basin.

The aim of the study is to (1) describe the kerogen content of the Namurian mudstones in the Widmerpool–Edale Gulf area; (2) establish the amount of variability in the kerogen content of the mudstones within a single marine band (E_{2a}); and (3) evaluate the prospectivity of the mudstones within the E_{2a} marine band in the Widmerpool–Edale Gulf area.

2. Namurian stratigraphy of the deposits in the Pennine Basin

The Pennines in the central UK comprise a dissected plateau (up to 600m) composed of an asymmetrical anticline with Carboniferous strata gently dipping to the east and more steeply to the west (Aitkenhead et al., 2002). During the Chadian–early Arundian and late Asbian–Brigantian, a SSE–NNW crustal extension caused a fragmentation of Early Palaeozoic deposits giving rise to a rifted topography of fault-bounded blocks interspersed with developing grabens and half-grabens including the Widmerpool and Edale Gulf (Gawthorpe, 1987; Lee, 1988). By the end of the Visean, rift-associated extension in the area was replaced by a regime of thermal sag and an epicontinental sea transgressed the Pennine Basin leaving only the Southern Uplands and the Wales-Brabant High emergent (Figure 1) (Leeder, 1982; Leeder and McMahon, 1988).

The Namurian was a period of prograding deltas in the Pennine Basin when the basin topography, created during the Visean, was gradually infilled. The sediments deposited during this stage correspond broadly to the Millstone Grit Group (Figure 3). Regular marine incursions punctuated the deltaic successions giving rise to a remarkable cyclicity: shale and/or dark-coloured limestone rich in marine fossils, typically goniatites (so-called ‘marine bands’), are overlain by shale and sandstone with fewer fossils (Gross et al., 2014; Holdsworth and Collinson, 1988; Martinsen et al., 1995). In the 13 million year span of the Namurian around 60 marine bands occur (Martinsen et al., 1995), 46 characterized by the occurrence of a key goniatite species (Bisat, 1923; Holdsworth and Collinson, 1988; Ramsbottom, 1977; Ramsbottom et al., 1962). The average duration of a marine band is estimated at 180 kyr, although considerable variation between the marine bands may occur (Maynard and Leeder, 1992).

For the Pendleian–Arnsbergian interval, marine band periodicities of 111 kyr have been estimated, and they are linked to an eccentricity forcing (Waters and Condon, 2012) of glacio-eustatic sea level fluctuations (Isbell et al., 2003; Stephenson et al., 2008; Veevers and Powell, 1987). Superimposed on these minor cycles, eleven longer duration, 1.1–1.35 myr, mesothems have been identified

(Ramsbottom, 1977). These mesothems are interpreted as longer term marine transgressions, characterized by the appearance of new ammonoid genera and each one capped by an extensive ammonoid band (Ramsbottom, 1979). In a sequence stratigraphic context, the marine bands can be thought of as parasequences representing the maximum flooding surfaces, while the mesothems correspond to sequences (Posamentier et al., 1988).

2.1 Visean–Namurian deposits in the Widmerpool and Edale Gulfs

The Visean–early Namurian Craven Group from the Widmerpool Gulf comprises the Long Eaton, Lockington Limestone and Widmerpool formations (Figure 3). The overlying Bowland Shale Formation, formerly termed the Edale Shales (Waters et al., 2009), commences at the base of the *Emstites leion* (E_{1a1}) (formerly *Cravenoceras leion*) Marine Band and has a highly diachronous upper boundary with the feldspathic sandstones typical of the Millstone Grit Group (Stevenson et al., 1971). The Bowland Shale Formation is a dark grey calcareous mudstone with thin turbiditic sandstones which in the southern part of the Pennine Basin, close to the northern margin of the Wales-Brabant High, passes over in the shaly mudstones and pale grey protoquartzitic siltstones of the Morridge Formation (Waters et al., 2009). The Morridge Formation is an early Namurian equivalent of the Millstone Grit Series (Figure 3) and was introduced by Waters et al. (2007) to reflect the predominantly southern provenance of the terrigeneous material making up the sandstone intervals: coarse quartz-feldspathic sediments derived from Greenland and Fennoscandia make up the terrigeneous component of the Millstone Grit Series (Drewery et al., 1987) while quartz-rich sediments in the sandstone intervals of the Morridge formation originate from the Wales-Brabant High (Trewin and Holdsworth, 1973).

The late Visean, Asbian and Brigantian, deposits in the Edale Gulf were described by Gutteridge (1991) and consist of the Ecton Limestone and Widmerpool Formations (Figure 3). The Namurian successions of the Derbyshire High–Edale Gulf are poorly understood as they are only described from the Alport and Edale Boreholes that were drilled in the late 1930s. During the late Brigantian–early Pendleian, carbonate production waned over the Derbyshire High and up to 356 m of mudstone-dominated successions of the Bowland Shale Formation were deposited ranging in age from

Pendleian to Kinderscoutian (Figure 3) (Waters et al., 2009). The lower part of the Bowland Shale Formation in the Edale Gulf consists of a succession of grey mudstone with thin beds of calcareous quartzose siltstones which may represent the distal delta-slope equivalent of the Morridge Formation (Waters et al., 2009).

2.2 The Carsington Dam Reconstruction Borehole C3

The Carsington Dam Reconstruction Borehole C3 (1.63°W; 53.05°N; Figure 2) was drilled in 1990 to assess fluid movements and pressures of the reconstructed Carsington Dam following its failure in 1984 (Skempton and Vaughan, 1993). In the palaeogeographic reconstruction of the Namurian, it is located close to the centre of the Widmerpool Gulf half graben (Figure 1). In total, 38 m of mudstones, siltstones, sandstones and limestones belonging to the Morridge Formation were cored across the E_{2a} *Cravenoceras cowlingense*, E_{2a3} *Eumorphoceras yatesae* and E_{2b1} *Cravenoceratoides edalensis* Marine Bands (Aitkenhead, 1991) (Figure 5). The E_{2a} and E_{2a3} bands are part of the N1 mesothem, while the E_{2a3}–E_{2b1} boundary forms the transition between the N1 and N2 mesothems (Aitkenhead, 1991).

2.3 The Karenight 1 Borehole

The Karenight 1 borehole (1.53°W; 53.18°N; Figure 2) was drilled as a mineral exploration borehole by Drilling and Prospecting International in 1973. It was drilled near the northern boundary of the Derbyshire High towards the Edale Gulf (Figure 1). The borehole was drilled to a terminal depth of 428.37 m and was cored below 59.59 m onwards (Wilson and Stevenson, 1973). In the current study we investigated the 234.70–251.89 m interval, consisting of mostly carbonate-cemented mudstone interspersed with limestone (250.93–244.5 m) and siltstone (244.5–234.70 m) (Figure 6). This interval comprises the upper part of the Pendleian Substage (E_1; 251.89–248.55 m) and the E_2 *Eumorphoceras* zone with the E_{2b} marine band tentatively recognized at 241.90m (Wilson and Stevenson, 1973).

3. Methodology

3.1 Palynological analysis

In total, the palynofacies composition of 55 samples assessed: 22 from the Carsington Dam Reconstruction C3 Borehole (Carsington DR C3) (Appendix 1) and 33 from the Karenight 1 Borehole (Appendix 2). Approximately 5 grams of each sample was processed at the British Geological Survey utilizing hydrochloric (36%) and hydrofluoric acid (40%) to eliminate carbonates and silicates. Samples were spiked with *Lycopodium clavatum* (Batch No. 3862) to enable concentration and flux calculations utilizing the marker grain method (Maher, 1981; Stockmarr, 1971). Subsequently, the kerogen fraction was sieved on a 10 μm nylon mesh and was strew-mounted on microslides using Elvacite™. Optical examination was performed using a Nikon Eclipse Ci-L microscope (400X magnification for routine study, 1000X for studying morphological details) equipped with a Prior H101A Motorized Stage that was controlled by a Prior™ Proscan III unit connected to a PC with the open source microscopy software μManager (https://micro-manager.org/wiki/Micro-Manager) preinstalled. Per sample, 300 particles were identified following the palynofacies classification of Tyson (1995) and using randomly generated slide positions. All slides were scanned for the presence of spores which were recorded separately from the palynofacies analyses. Furthermore, we studied the slides using blue light excitation (near UV) on a Zeiss Universal microscope operating in incident-light excitation mode with a III RS condenser set and the Zeiss filter set 09 (exciter filter: 450–490 nm; chromatic beam splitter: 510 nm; barrier filter: 515–565 nm). We followed the standard recommendations for epifluorescence observations on palynological slides (Tyson ,1995; Tyson, 2006). Images of palynomorphs (Plates 1–2) in transmitted white light were taken with a Nikon DS-Fi3 camera mounted on the Nikon Eclipse Ci-L microscope and the NIS Elements™ microscope imaging software.

3.2 Rock-Eval^{TM} Pyrolysis

In total 169 samples were analysed from Carsington DR C3 (Appendix 3) and 72 samples from Karenight 1 (Appendix 4) using a Rock-Eval^{TM} (6) analyser configured in standard mode. Freeze dried, powdered samples (60 mg/dry wt) were heated at 300°C for 3 minutes and then heated from 300°C to 650°C at 25°C/min in N_2 atmosphere and the residual carbon oxidised at 300°C to 850°C at 20°C/min. Hydrocarbons released during the two-stage pyrolysis were measured using a flame ionization detector (FID) and CO and CO_2 measured using an infra-red (IR) cell. Rock-Eval parameters were calculated by integration of the amounts of hydrocarbon (HC), thermally-vaporized free hydrocarbons, expressed in mg HC/g rock (S_1) and hydrocarbons released from cracking of bound OM expressed in mg HC/g rock (S_2). The Hydrogen Index (HI) and Oxygen Index (OI) were calculated following Newell et al. (2016) and Słowakiewicz et al. (2015) and expressed in mg/g TOC:

$$HI_{pd} = \frac{S_2 * 100}{TOC_{pd}} \quad (1)$$

$$OI_{pd} = \frac{S_3 * 100}{TOC_{pd}} \quad (2)$$

Thermal maxima values (T_{max}) were determined from the highest yield of bound hydrocarbons (S_2). The performance of the instrument was checked every 8 samples against the accepted values of the Institut Français du Pétrole (IFP) standard (IFP 160 000, S/N1 5-081840) and instrumental error (standard deviation) was S_1±0.1 mg HC/g rock, S_2 ±0.77 mg HC/g rock, TOC ±0.04% wt, Mineral C ± 0.04% wt, T_{max} ±1.4°C.

3.3 X-ray diffraction analysis

The mineralogy of 17 samples from Carsington DR C3 (Appendix 5) and 10 samples from Karenight 1 (Appendix 6) was determined by quantitative X-ray diffraction (XRD) analysis. Samples were analysed using a PANalytical™ X'Pert Pro series diffractometer equipped with a cobalt-target tube, X'Celerator detector and operated at 45kV and 40mA. Whole-rock analysis was carried out on spray-dried, micronised powders which were scanned from 4.5-85°2θ at 2.06°2θ/minute. Mineral phases were identified using PANalytical™ X'Pert HighScore Plus version 4.5 software coupled to the latest version of the International Centre for Diffraction Data (ICDD) database. Quantification was achieved by using the Rietveld refinement technique (e.g. Snyder & Bish, 1989) with the same HighScore™ Plus software and reference files from the Inorganic Crystal Structural Database (ICSD).

The clay mineralogy of the samples (Appendices 7, 8) was determined using a broadly similar approach to that detailed in Kemp et al. (2016). Where whole-rock XRD analysis indicated that the samples were composed of substantial amounts of carbonate species, these were removed using a buffered sodium acetate/acetic acid (pH 5.3). For this study <2 µm fractions were isolated, oriented mounts prepared and scanned from 2-40°2θ at 1.02°2θ/minute after air-drying, ethylene glycol-solvation (16 hours) and heating at 550°C (2 hours). Clay mineral species were then identified from their characteristic peak positions and intensities and their reaction to the diagnostic testing program.

Further clay mineral characterisation and quantitative evaluation was carried out using Newmod II™ software (Reynolds & Reynolds, 2013) modelling of the glycol-solvated XRD profiles on all the samples.

3.4 Organic carbon isotope composition ($\delta^{13}C_{OM}$)

We determined the organic carbon isotope composition ($\delta^{13}C_{OM}$) from 30 Carsington DR C3 samples (Appendix 9) and from 57 Karenight 1 samples (Appendix 10). $^{13}C/^{12}C$ analyses were performed by combustion in a Costech Elemental Analyser (EA) on-line to a VG TripleTrap and Optima dual-inlet mass spectrometer, with $\delta^{13}C_{OM}$ values calculated to the VPDB scale using a within-run laboratory standards calibrated against NBS18, NBS-19 and NBS-22. Replicate analysis of well-mixed samples indicated a precision of $\pm$ <0.1‰ (1 SD).

4. Results

The palynofacies analysis, Rock-Eval^{TM} and $\delta^{13}C_{OM}$ and XRD results are presented below and are summarized in the Appendices 1–10. The palynofacies analyses was conducted on samples that were also used for geochemical (Rock-Eval^{TM} and $\delta^{13}C_{OM}$) analyses. Additional samples were collected for XRD analyses.

4.1 Palynofacies analysis

The palynofacies assessment follows the palynological kerogen classification of Tyson (1995). Structureless (heterogeneous + homogeneous) amorphous organic matter (AOM) was distinguished from structured material (phytoclasts, sporomorphs, phytoplankton, fungal remains) and any residual mineral matter, mainly pyrite, which was not eliminated during sample preparation.

4.1.1 Carsington DR C3

The palynological analysis of the 22 Carsington DR C3 samples is summarized in Appendix 1 and Figure 5. Structureless organic constituents dominate the kerogen fractions making up on average 86% the counts with a minimum of 74% (SSK45636; 31.61 m) and a maximum of 95% (SSK45607; 26.18 m). Within this structureless category, heterogeneous AOM (Plate I, Figure 1–4) with grumose AOM (Plate I, Figure 1) as the most important constituent is the dominant organic category averaging 62% of the counts, with a minimum of 19% (SSK46355; 53.57 m) and a maximum of 86%

(SSK46331; 46.08 m). Homogeneous AOM, with gelified organic matter as the dominant constituent (Plate I, Figure 5), forms on average 25% of the kerogen fraction, with a minimum of 4% (SSK45621; 28.94 m) and a maximum of 60% (MPA65588; 53.57 m). The abundance of homogeneous AOM surpasses the abundance of heterogeneous AOM in four samples: SSK46355 (53.57 m), SSK46311 (42.58 m), SSK45634 (31.11 m) and SSK45616 (28.22 m).

Within the structured organic material, phytoclasts are the most abundant organic constituent averaging about 8% of the counts with a minimum of 2% (SSK45607; 26.18 m) and a maximum of 22% (SSK46301; 40.83 m). Phytoclasts (Plate I, Figure 5, black arrow) are especially abundant below the E_{2a}3 Marine Band. Palynomorphs are rare throughout the section averaging 4% with a minimum below 1% in SSK46311 (42.58m) and a maximum of 14% in SSK46351 (51.86m). Sporomorphs are the most important palynomorph type. *Lycospora pusilla* (Plate II, Figure 1) is the most common identified spore with minor abundances of *Cingulizonates bialatus* (Plate II, Figure 2), *Granulatisporites granulatus* (Plate II, Figure 3), *Savitrisporites nux* (Plate II, Figure 4), *Densosporites anulatus* (Plate II, Figure 5) and *Crassispora kosankei* (Plate II, Figure 6).

4.1.2 Karenight 1

The palynological analysis of the 33 samples of Karenight 1 is summarized in Appendix 2 and Figure 6. Structureless organic constituents dominate all Karenight 1 samples (as with the Carsington DR C3 results), averaging a relative abundance of 88% with a minimum of 72% (SSK53146; 251.89 m) and a maximum of 97% (SSK51212; 245.50 m). Heterogeneous AOM is the dominant category of structureless material with on average a relative abundance of 77% (minimum 58% in SSK53146 at 251.89 m; maximum 94% in SSK51212 at 245.50 m). Homogeneous AOM, mostly composed of gelified matter and AOM in a gelified matrix, has an average relative abundance of 11% with a minimum of 3% recorded in SSK51212 (245.50 m) and a maximum of 24% in SSK51202 (243.28 m). The relative abundances of homogeneous AOM are noticeably less than the relative abundances of heterogeneous AOM. The average abundance of heterogeneous-homogeneous AOM is 66% with a minimum of 39% in SSK51180 (237.90 m) and a maximum of 91% in SSK5121 (245.50 m).

Phytoclasts comprise the most abundant structured organic constituent with a relative abundance of 7% (maximum of 22% in SSK53146 at 251.89 m; minimum of <1% in SSK46369 at 235.98 m and SSK51182 at 238.46 m). The highest phytoclast abundances are reached during the Pendleian (E_1). Palynomorphs are very sparse in the Karenight 1 section averaging only 1% (maximum of 5% in SSK51192 at 240.93 m and SSK53146 at 251.89 m) including five samples where no palynomorphs were recorded in 300 fields of view (SSK53135, SSK52580, SSK51208, SSK51204, SSK51182). Spores are the most common discrete palynomorphs, with poor preservation causing most to remain unidentified. *Lycospora pusilla* is again the most common identified spore with minor occurrences of *Granulatisporites granulatus, Florinites* spp. and *Cingulizonates bialatus*.

4.2 Geochemical analyses: Rock-Eval^{TM} pyrolysis and $\delta^{13}C_{OM}$

4.2.1 Carsington DR C3

Nine Rock-Eval^{TM} parameters (S_1, S_2, S_3, HI_{pd} (present day Hydrogen Index), OI, T_{max}, TOC_{pd} (present day Total Organic Carbon), Remnant Carbon (RC) and Pyrolised Carbon (PC)) for 169 samples are summarized in Appendix 3 and 30 measurements of $\delta^{13}C_{OM}$ in Appendix 9. In Figure 5 we show TOC_{pd}, PC, S_1, T_{max}, HI_{pd} and $\delta^{13}C_{OM}$ data alongside the sedimentological log. For the E_{2a} zone up to E_{2a3}, TOC_{pd} and PC are relatively low, with TOC_{pd} values averaging 1.95% (with a minimum of 0.21% at 45.28 m and a maximum of 5.16% at 48.60%, while PC averages 0.33 with a minimum of 0.02% at 31.11 m and a maximum of 1.02% at 43.33 m. The TOC_{pd} (and PC) are higher in the E_{2a3} and E_{2b1} marine bands with TOC_{pd} reaching an average of 3.52% with a maximum of 5.52% at 24.23 m and a minimum of 0.5% while PC averages 0.77% with a minimum of 0.06% at 20.10 m and a maximum of 1.66% at 25.68 m.

The HI_{pd} of the section from E_{2a} to the E_{2a3} boundary averages 162 mg/g TOC_{pd}, with a minimum of 28 mg/g TOC_{pd} at 34.28 m and a maximum of 428 mg/g TOC_{pd} at 38.77 m. For the upper part of the studied section HI_{pd} averages 228 mg/g TOC_{pd} with a minimum of 81 mg/g TOC_{pd} at 27.08 m and a maximum of 366 mg/g TOC_{pd} at 26.78 m.

The E_{2a}–E_{2a3} boundary is also coeval with an uphole rise in S_1: the S_1 diagram with an average of 0.19 mg/g for the lower part (minimum of 0.01 mg/g at 34.28 m; maximum of 1.28 mg/g at 33.72 m) and an average of 0.54 mg/g (minimum of 0.04 mg/g at 20.10 m; maximum of 1.01 at 25.68 m).

The T_{max} remains relatively constant throughout the entire interval averaging 435°C. Only in the sandstone and siltstone interval around 34 m a drop in T_{max} to a minimum of 366°C has been recorded.

The $\delta^{13}C_{OM}$ data follow the trend of TOC_{pd} and S_1 with higher values in the lower part of the section (55.46–25.40 m) averaging -26.2‰ (with a minimum of -28.7‰ and a maximum of -24.0‰). In the upper part of the section (25.40–18.44 m), $\delta^{13}C_{OM}$ average -28.0‰ (with a minimum of -30.0‰ and a maximum of -25.0‰).

4.2.1 Karenight 1

Nine Rock-Eval™ parameters (S_1, S_2, S_3, HI_{pd}, OI, T_{max}, TOC_{pd}, RC and PC are summarized in Appendix 4 and $\delta^{13}C_{OM}$ in Appendix 10). In Figure 6 we show the TOC_{pd}, PC, S_1, T_{max} and HI_{pd} and $\delta^{13}C_{OM}$ data alongside the sedimentological log. The Rock-Eval™ parameters show a drop around 242 m near the base of the tentative E_{2b} zone. The TOC_{pd} of mudstone in the lower part of the section averages 7.01% with a minimum of 4.32% at 251.61 m and a maximum of 9.29% at 249.22 m, while PC of the mudstones averages 1.42% (minimum of 0.74% at 245.8 m; maximum of 2.42% at 249.22 m). Limestone of the lower section has a much lower carbon content than the mudstone. The TOC_{pd} of the three recovered limestone samples averages 0.84% (with a minimum of 0.36% at 251.1m and a maximum of 1.09% at 248.93 m), and the RC averages only 0.17% (with a minimum of 0.07% at 251.1 m and a maximum of 0.22% at 248.93 m and 247.1 m).

The TOC_{pd} of the upper part of the section between 242.80–234.77 m is significantly less than the TOC_{pd} of the lower part, averaging 3.94% with a minimum of 1.65% at 242.15 m and a maximum of 7.08% at 236.66 m. The PC values are low with an average of 0.71%, a minimum of 0.20% at 242.15 m and a maximum of 1.75% at 236.66 m.

The $\delta^{13}C_{OM}$ data follow the trend of TOC_{pd} and S_1 with lower values in the 251.89–242.80 m interval, averaging -28.4‰ with a minimum of -29.1‰ and a maximum of -26.7‰. In the upper part of the section, between 242.80–234.77 m, $\delta^{13}C_{OM}$ average -27.6‰ with a minimum of -29.5‰ and a maximum of -25.6‰.

The HI_{pd} and T_{max} curves follow this trend: from 251.89 to 242.80 m: low and relatively consistent HI_{pd} values, 108 mg/g TOC (217 mg/g TOC) 260 mg/g TOC and lower T_{max}, 424 °C (431 °C) 442 °C. From 242.80 to 234.80 m: low values for HI_{pd}, 82 mg/g TOC (183 mg/g TOC) 293 mg/g TOC, and T_{max}, 425 °C (433 °C) 440 °C.

4.3 Mineralogical analysis

The whole-rock and <2 µm clay mineral XRD analyses for 17 samples from Carsington DR C3 are summarized in Appendices 5 and 7. The XRD analyses for 10 samples from Karenight 1 are summarized in Appendices 6 and 8. Results from both boreholes are summarized in the ternary mudstone classification diagram of Figure 8.

4.3.1 Carsington DR C3

Thirteen samples originate from the bottom part of the section (E_{2a} below E_{2a3}; 53.57–28.22 m) which all plot in the siliceous and argillaceous mudstone fields. These samples are generally carbonate-free with only a single sample containing minor amounts of rhodocrosite (1.6% at 40.83 m). Silicates (quartz with rare plagioclase feldspar) dominate the composition with on average 41%, with a maximum of 83.6% (33.63 m) and a minimum of 23.6% (43.26 m). Pyrite forms up to 7.6% of these samples and the oxidation products jarosite and gypsum were also detected. The phyllosilicate/clay mineral assemblages of the E_{2a} samples are dominated by undifferentiated 'mica' species (including muscovite, biotite, illite and illite/smectite (I/S)) with minor amounts of kaolinite and traces of chlorite. Less than 2 µm analyses and Newmod II-modelling confirm this assemblage and subdivided the 'mica' into discrete illite and an *R*1-ordered I/S containing 80% illite interlayers.

The remaining four samples (E_{2a3} and E_{2b1}; 18.44–26.18 m) all plot in the siliceous mudstone field. These samples are characterized by a higher carbonate (calcite, dolomite, Fe dolomite/ankerite) content (on average 7.63%) and a maximum of 24.2% in the lowermost sample (26.18m). These samples are also pyritic but are less phyllosilicate/clay mineral-rich than the underlying samples. Although the detected clay minerals in the <2 µm fractions are similar to the shales below E_{2a3}, they noticeably contain a lower proportion of kaolinite and chlorite and higher proportions of I/S and illite.

4.3.2 Karenight 1

The lowermost six samples 251.84–242.98 m interval (E_1–E_{2b}?) plot in the argillaceous mudstone and siliceous mudstone fields. While low, the carbonate content of this interval is higher than in the bottom part of Carsington DR C3 averaging 4.7% with a maximum of 10.7% at 251.84 m. The four samples from the top part of the section (E_{2b}?; 236.07–242.32 m) are generally richer in carbonates (calcite and dolomite, averaging 28.5%) with a maximum of 49.4% at 238.33 m. This sample plots in the mudstone field of Figure 8.

Less than 2 µm XRD analyses suggest *R*1 (80% illite) I/S- and illite-dominated clay mineral assemblages with only traces of kaolinite and chlorite, similar to those identified in the upper interval of the Carsington DR C3 borehole.

5. Discussion

To assess the shale gas prospectivity of the Widmerpool Gulf and Edale Gulf we apply the criteria detailed in Table 2 of Andrews (2013). With the data generated in the current study we can expand the UK data set and discuss four criteria in more detail (Table 1): organic matter content (and original TOC, TOC_o), kerogen type, original hydrogen index (HI_o), mineralogy and clay content.

5.1 Organic matter content (TOC)

The TOC_{pd} or organic richness of a potential source rock was measured using Rock-Eval™ pyrolysis and is reported in dry weight percent. Because organic matter generates hydrocarbons during maturation, TOC_{pd} is generally viewed as an important variable that has a strong influence on the amount of potential hydrocarbons that can be generated. Even though there is consensus that a potential source rock should be rich in organic matter and TOC_{pd} can serve as a proxy for that, reported cut-off values vary from basin to basin and from author to author: e.g. >2% (Gilman and Robinson, 2011; TNO, 2009), >4% (Lewis et al., 2004). For the Carboniferous Pennine Basin, Andrews (2013) utilizes a TOC_{pd} cut-off of 2% to screen potentially viable shale horizons. However, it is important to acknowledge that measured values relate to TOC_{pd} composed of the pyrolysable fraction of the organic carbon (PC) and the remaining carbon after pyrolysis (RC) (Figure 9). The PC represents the present day generative part (GOC_{pd}) while the RC represents the present day non-generative part of the organic carbon ($NGOC_{pd}$) of the sample that was subjected to Rock-Eval pyrolysis. From the moment of sampling to the acquisition of the pyrolysis results, losses of organic carbon occur due to storage, handling and sample processing. Losses also occur due to natural processes associated with basin evolution, including diagenesis and maturation of the sediments and due to migration of formed hydrocarbons (Figure 9). As a result, the original TOC (TOC_o) is composed of the original GOC (GOC_o) and the original NGOC ($NGOC_o$). Jarvie (2012) provides a methodology to calculate TOC_o (see paragraph 5.2) and uses a cut-off value of 1% TOC_o as a criterion for prospective shale plays. Thus, the interpretation of TOC values relies on the assumption that the loss of carbon from deposition to analysis is not biased towards GOC or its components, and quantitatively similar for all compared samples. While this may be a reasonable assumption for a set of samples from the same bed, TOC_{pd} can vary by as much as 10% within the same shale system (Figure 7 in Jarvie, 2012) which draws into doubt the validity of inter-basinal comparisons of TOC values. Indeed, some techniques that rely on indirect estimates of the OM component to estimate shale gas resource, such as the Passey Method (Passey et al., 1990) applied to down-hole geophysical logs, may give unrealistically high estimates of gas generative potential.

In the Carsington DR C3 core 142 of a total of 169 samples have TOC_{pd} values above 1% and 97 samples have TOC_{pd} higher than 2% (Appendix 3). Biozones E_{2b1} and E_{2a3} (18.02–27.32 m) have the highest TOC_{pd} with only the thin limestone bed at 20.10 m containing less than 1% organic carbon. However when PC is considered, values are much lower and only 7 samples, 6 of which originating from the E_{2b1}–E_{2a3} interval, show higher than 1% PC and no samples exceed 2% PC. In conclusion, the majority of the Carsington DR C3 samples meet the >2% criterion of Andrews (2013) for TOC values of a prospective shale interval, especially in the E_{2b1} and E_{2a3} and only in restricted intervals in the rest of the studied interval. When PC is considered, no samples exceed the 2% threshold.

In the Karenight 1 core, 71 of a total of 72 samples have TOC_{pd} higher than 1% and 68 have TOC_{pd} higher than 2% (Appendix 4). The only samples that do not meet the 2% requirement are limestone that are present throughout the interval. When PC is considered, only 38 samples surpass 1%, concentrated in the lower part of the core, and only 3 samples exceed 2%.

5.2 Kerogen type, original HI (HI_o) and original TOC (TOC_o)

The palynofacies analyses are based on the classification of Tyson (1995) and are summarized in Appendix 1 (Carsington DR C3) and Appendix 2 (Karenight 1) and on a AOM–Phytoclast–Palynomorph (APP) plot (Figure 7). Kerogen typing follows the summary given in Table 2 following Tyson (1995). The kerogen types encountered in the two boreholes studied here correspond broadly with the tentative kerogen typing for the Widmerpool and Edale Gulf by Ewbank et al. (1993). Mudstone contains higher percentages of Type II kerogen while coarser-grained intervals are richer in Type III. There is very little evidence of algal material (even though *Botryococcus* specimens were recorded in the upper part of Carsington DRC3; Plate I, Figure 6) and phytoplankton in the samples, a common observation in the Late Palaeozoic, dubbed as the Late Palaeozoic phytoplankton blackout (Riegel, 2008). Heterogeneous amorphous organic matter seems a likely candidate to represent these cryptic fossil groups. This has potentially important consequences for the typing of kerogen materials and the subsequent assessment of the prospectivity of source rocks. It is possible that a proportion of the heterogeneous AOM can be considered as Type I. In addition to transmitted white light, all samples were scanned using near-UV blue light and scored following Tyson's qualitative fluorescence scale (FS) (Table 20.2 in Tyson, 1995). Figure 7 shows that samples rich in heterogeneous AOM generally exhibit stronger fluorescence. The fluorescent compounds, fluorophors, are carotenoids of sporinite, isoprenoids of alginite and the phenols of cutinite and suberinite (Lin and Davis, 1988). Hydrocarbon potential and fluorescence are closely related (Van Gijzel, 1982) as fluorescence is enhanced when these compounds are distributed in an aliphatic environment (Robert, 1988). Using the relative abundances of AOM and phytoclasts, the qualitative fluorescence scale, a fluorescence scale index (FSI) can be calculated (Tyson, 2006):

$$FSI = FS \times \left(\frac{AOM}{AOM+Phyto}\right) \tag{3}$$

Where FS is the fluorescence scale, AOM is the relative abundance of amorphous organic matter and Phyto represents the relative abundance of phytoclasts. The maximum value for FSI is 6, when the maximum of FS = 6 is reached in a sample where the palynological counts reach 100% AOM. Therefore, to have an estimate of how much of the heterogeneous AOM consists of the highly fluorescent algal material, and therefore Type I kerogen, we divided the acquired FSI by 6 and multiplied it with relative abundance of heterogeneous AOM. This provides an estimate of the abundance of highly fluorescent AOM. The remainder of the fraction of heterogeneous AOM was regarded as Type II kerogen. It is possible that this fraction of low fluorescing, heterogeneous AOM was formed through bacterial modification of plant material, a class which other authors (Horsfield, 1984; Cooper and Barnard, 1984; Tyson, 1995) also tabulated under Type II kerogen. The final kerogen typing used for subsequent calculation is summarized in Table 3 (Carsington DR C3) and Table 4 (Karenight) and were used in the HI_o equation of Jarvie et al. (2007):

$$HI_0 = \left(\frac{\%\,type\,I}{100} \times 750\right) + \left(\frac{\%\,type\,II}{100} \times 450\right) + \left(\frac{\%\,type\,III}{100} \times 125\right) + \left(\frac{\%\,type\,IV}{100} \times 50\right) \quad (4)$$

The HI_o results from the Carsington DR C3 Borehole are summarized in Table 3.

Using the HI_o, the original TOC (TOC_o) can be calculated following Jarvie (2012):

$$TOC_o = \frac{\left[TOC_{pd} - \left(0.085 \times \left(S1_{pd} + S2_{pd}\right)\right)\right] - \left(HI_o \times 0.0008\right)}{\left(1 - HI_o/1177\right)} \quad (5)$$

Overall, the samples of Carsington DR C3 have an average HI_o of 409 mg/g TOC_o and an average TOC_o of 2.28% (Table 3). The geochemical trends observed from HI_{pd} and TOC_{pd} measurements are maintained. Downhole, the E_{2b1}–E_{2a3} interval shows higher HI_o and TOC_o values (465 mg/g TOC and 3.20% respectively) compared to the remainder of the E_{2a} interval (396 mg/g TOC and 1.04% respectively).

The HI_o and TOC_o results from the Karenight 1 Borehole are shown in Table 4. Both HI_o and TOC_o show a similar pattern as the present day values obtained by analysis and shown in Figure 6. The average HI_o value in the Karenight 1 Borehole is relatively stable throughout: 352 mg/g TOC_o (479 mg/g TOC_o) 607 mg/g TOC_o. The upper part of the studied section (242.48–234.77m) shows lower

HI_o and TOC_o values averaging 448 mg/g TOC_o 4.43% respectively. The lower part of the section (251.89–242.48 m) shows an average HI_o of 504 mg/g TOC_o with an average TOC_o of 9.34%. The interval from 243.67 to 245.50 m is notable in that it is characterized by a relatively high average TOC_o of 12.11%.

5.3 Mineralogy, clay content and maturity

The XRD results are plotted as a ternary diagram with carbonates, clay and silicates as end members with the results of similar analyses from producing North American shale reservoirs (Figure 8) and the ductile-brittle transition zone from Anderson (2014). Jarvie (2012) suggests a clay content <35%, a silicate content exceeding 30% with some carbonates and the presence of non-swelling clays is required to enable hydraulic fracturing. This is again based on observations from the Barnett Shale and there are examples of productive shales with higher clay contents (e.g. Sone and Zoback, 2013). Indeed, even plastic clays will hydrofracture if the pressurization rate is high enough (Cuss et al., 2015).

The upper part of the Carsington DR C3 borehole (18.44–27.60 m) is dominantly a siliceous mudstone with a variable carbonate content (up to 24%). On average, these samples contain 28% clay minerals. In contrast, the lower part of Carsington DR C3 (27.60–55.46 m) is generally carbonate-free and higher clay content (57% on average). Hence, this interval is considered an argillaceous mudstone.

The upper part of the Karenight 1 borehole (236.07–242.32 m) consists of argillaceous and siliceous mudstones with a considerable carbonate content (maximum 49%) and a relitively high clay content (25–55%). Calcite is most commonly developed with the exception of SSK59376 (236.07 m) which has a dolomitic content of 27% (Appendix 6).The lower part of Karenight 1 (242.98–251.84 m) consists of siliceous and argillaceous mudstone with a low carbonate content (maximum 10%) and a clay content 32–58%.

These results indicate the high variability of the mudstone mineralogy in both the Widmerpool and Edale gulfs. The same subdivisions that became apparent in the geochemical parameters (Figures 5 and 6) are reflected in the XRD analyses. A knowledge of the clay mineralogy of these mudstones is important in determining their potential engineering behaviour (Jarvie, 2012). No discrete smectite, the most common high shrink-swell clay mineral, was identified in either of the borehole intervals examined. However, the ubiquitous presence of *R*1-ordered I/S (80% illite, 20% smectite) should be noted and influence the design of any hydraulic fracture programmes.

In addition, clay minerals can also provide a geothermometer for comparison with more traditional organic maturation indices, as illustrated by the Basin Maturity Chart of Merriman & Kemp, (1996). The consistent presence of *R*1-ordered I/S (80% illite, 20% smectite) in borehole intervals suggests burial temperatures of ~100°C and places the formation in the Late (or Deep) Diagenetic metapelitic zone, equivalent to burial of perhaps 4 km at normal geothermal gradients (~25°C/km). In terms of hydrocarbon zones, the clay data suggest light oil maturity. This is consistent with the acquired Rock Eval parameters for both studied intervals. The T_{max} values in the Carsington DR C3 interval remains constant around 430–440 ºC (Figure 5), showing a uniform maturity near the bottom of the oil window (435–470 ºC). Only the sandstone interval between 33.50–34.75 m shows a drop in T_{max} to 366 ºC. The bulk organic matter in this interval is from a distinctively different origin than the rest of the interval: sample SSK45647 at 33.63 m has the lowest recorded HI_{pd} and a low FS of 2. Hence, the T_{max} variations in this instance can be attributed to the origin of the organic matter rather than a change in maturity. In the Karenight 1 core, T_{max} averages 435 ºC and remains in the narrow interval 424–445 ºC over the entire studied interval, averaging 435 ºC. There is an increase of about 10 ºC in T_{max} occurring around 245.70 m below the lowest occurrence of visible plant material in the core. The lithological composition, the fossil content and the occurrence of some of the most negative $\delta^{13}C_{OM}$ values (see Section 5.4) all point to a more marine depositional environment. Therefore we attribute the minor change in T_{max} at 245.70 m to the nature of the organic matter rather than to a change in maturity.

5.4 Organic matter $\delta^{13}C_{OM}$

Peters-Kottig et al. (2006) investigated long and short term variations in $\delta^{13}C_{OM}$ that occur in land plant organic matter in the late Palaeozoic. The rise of land plants during the Carboniferous and the Permian has been related to the drawdown of atmospheric CO_2 and the initiation of glacial episodes

(Kump et al., 2000). This is linked to the rise in importance of lycophytes during the Serpukhovian (Cleal and Thomas, 2005); these plants were very efficient carbon sinks, large in size and they possessed photosynthetic leaf cushion covered stems and leafs (Phillips and diMichele, 1990; Thomas, 1978). Carbon burial during the late Mississippian was exacerbated by the widespread lignin production since the late Devonian (Robinson, 1990), leading to increased burial of organic matter resulting in a further CO_2 drawdown and a large pO_2 peak around 300 Ma and thus a lower $\delta^{13}C_{OM}$ signature of the plant material as the Mississippian advanced (Berner et al., 2000) to values of around -25‰ (Peters-Kottig et al., 2006). Even though extant marine plants are generally characterised by higher $\delta^{13}C_{OM}$ values than land plants (Craig, 1953; Silverman and Epstein 1958), $\delta^{13}C_{OM}$ measurements of marine kerogen are generally lower than terrestrial kerogen (e.g. Newman et al., 1973). This was confirmed for Mississippian shales of the Appalachian Basin where terrigenous organic matter has $\delta^{13}C_{OM}$ of -26 to -25‰ while the $\delta^{13}C_{OM}$ of the marine organic matter is around -30‰ (Maynard, 1981). Lewan (1986) evaluated $\delta^{13}C_{OM}$ values of amorphous kerogens in Phanerozoic sediments and distinguished ‘h’ amorphous kerogens (-24 to -26‰) from ‘l’ amorphous kerogens (-35 to -26‰). Phytoplankton residing in environments with well-circulated water masses dominated by atmospheric-derived CO_2 will yield ‘h’ amorphous kerogen while ‘l’ amorphous kerogens were more likely formed in more restricted basins overlain by relatively shallow, well-stratified water masses where carbon in the photic zone is sourced from recycled organic material (Lewan, 1986).

These principles can be applied to the Mississippian deposits of the Pennine Basin, where the kerogen fraction is dominated by AOM (Figures 5–7, Appendix 1–2). The contrasting $\delta^{13}C_{OM}$ values between terrestrial and marine kerogen can be used to delimit marine and non-marine intervals. Stephenson et al. (2008; 2010) showed that the bulk $\delta^{13}C$ values of the mixed marine-terrestrial sequence in the Throckley and Rowland Gill boreholes is a function of the ratio marine:terrestrial $\delta^{13}C_{OM}$. Similarly, Könitzer et al. (2014), demonstrated the influences of microfacies, organic matter source and biological activity in a cross plot of $\delta^{13}C_{OM}$ and TOC for deposits of the Carsington DR C4 Borehole, which covers the same stratigraphic interval considered in the current study. In Figure 10 the Karenight 1 and Carsington DR C3 $\delta^{13}C_{OM}$ and TOC values are shown. The lower part of the

Carsington DR C3 core, corresponding to the E_{2a} biozone contains the lowest TOC and variable $\delta^{13}C_{OM}$ values. The highest $\delta^{13}C_{OM}$ values correspond with intervals where sandstone and siltstone, most likely deposited as turbiditic flows in the Widmerpool Gulf (Könitzer et al., 2014), carried more terrestrially sourced organic matter in the basin: around 54 m, 41–44 m, 34 m and 31 m. The isotope signature of the interspersed mudstones is lower and more marine-derived organic matter is incorporated in these sediments. The upper part of the Carsington DR C3 (biozones E_{2a3} and E_{2b1}) shows the influence of increased marine organic matter on the kerogen fraction. There are two outliers: at 20.10 m a limestone (SSK45591) has the lowest recorded $\delta^{13}C_{OM}$ value (-30‰) combined with the lowest TOC value (0.32 %). Limestone is characterised by a very low kerogen content and due to the depositional environment, what little kerogen there is, consists almost entirely of marine sourced organic matter. The other outlier is sample SSK45602 which has a relatively high $\delta^{13}C_{OM}$ value of -25‰. Despite the marine character of the lithology (silty mudstone), some plant fossils were recovered (Figure 5) from the interval which could explain the terrestrial nature of the $\delta^{13}C_{OM}$ signal. The lower part of the Karenight core (242.80–251.89 m) displays the lowest $\delta^{13}C_{OM}$ combined with the highest TOC values, reflecting the marine influence in this part of the section. The upper part contains a mix of marine derived kerogen, around 237–238 m and 240 m, interspersed with intervals containing more terrestrially derived kerogen, 236–237 m. Relatively, the Karenight 1 samples contain a higher abundance of marine kerogen compared to the Carsington DR C3 samples.

6. The prospectivity of the Arnsbergian (late Mississippian) shales of the Widmerpool and Edale Gulf

During the Mississippian (359–323.2 Ma) the Pennine Basin was located close to the equator, proximal to Laurussia with Gondwana stretching to the South Pole (McKerrow and Scotese, 1990) and it was bordered by two emerging land masses; the Southern Uplands to the north and the Wales-Brabant High to the south (Figure 1). Because of its position, ice sheets were likely to persist on Gondwana (Isbell et al., 2003) which influenced the sedimentation history in the patchwork of sub-basins forming the Pennine Basin (e.g. Stephenson et al., 2010). These sea level fluctuations most likely exerted less of an impact on the contemporaneous Upper Barnett Shales (Figure 3), deposited in the much more distally located Fort Worth Basin and one of the world's most prolific shale gas plays with an estimated resource of 43 tcf (US Energy Information Administration, 2011), than the mudstones considered in the current study.

The Fort Worth Basin was formed as a foreland basin in response to the collision of North and South America during the formation of Pangea (Walper, 1982) and its more distal position means the five lithofacies that are generally recognized in the Barnett Shale – i.e. black shale, lime grainstone, calcareous black shale, dolomitic black shale and phosphatic black shale (Loucks and Ruppel, 2007; Montgomery et al., 2005; Pollastro, 2003) – lack the turbidites that were encountered in the Carsington DR C3 core and the siltstones in the Karenight 1 core of the current study and indeed in most of the Namurian cycles in the Pennine Basin (Aitkenhead et al., 2002; Andrews, 2013). The more continuous nature of marine deposits of the Fort Worth Basin compared to the mudstone and turbidite successions of the Pennine Basin, reflects the respective position of both basins: the glacio-eustatic sea level fluctuations most likely exerted less of an impact on the contemporaneous Upper Barnett Shales deposited in the much more distally located Fort Worth Basin, than the mudstones considered in the current study. Most of the prospectivity criteria that were used to evaluate the Namurian shales from the UK, summarized in Table 1 and discussed in Sections 6.1–6.3, are based on observations from the Barnett Shale (see also Andrews, 2013; Jarvie, 2012).

6.1 Carsington DR C3

The Carsington DR C3 samples cover the E_{2a}, E_{2a3} and E_{2b1} marine bands (Figure 5).The lower part of the studied interval corresponds to the E_{2a} marine band below E_{2a3}. The TOC_{pd} of the mudstones of this interval is comparatively low (2% on average). There is variation in the TOC_{pd} with some intervals (32.50–34.50 m and 40.5–44 m) characterized by a low TOC_{pd} while some intervals (for example, around 37 m and 47–50 m) have a TOC_{pd} that surpasses 2.5%. However, the pyrolysable content of none of these samples surpasses the 2% constraint that is required for an unconventional gas reservoir (Andrews, 2013; Gilman and Robinson, 2011; TNO, 2009). The kerogen fraction contains a high calculated average of 70% Type II (Table 3), with an important contribution (7.8%) of Type III organic matter. The HI_o for this interval averages 468mg/g TOC falling in the prospective window of 250–800 mg/g TOC defined by Jarvie (2012) with an associated TOC_o of 2.28% on average. It should be noted that there is a considerable amount of variability in the TOC_o values throughout, with a minimum of 0.46% (SSK45632 at 30.89 m) and a maximum of 4.79% (SSK46019 at 37.10 m). The XRD analyses show there is a very low amount of carbonate contained in the lower part of Carsington DR C3 and a highly variable amount of silicates. Most samples are considered as argillaceous mudstones while three samples contain enough silicates to be classified as siliceous mudstones (Figure 8).

The upper part of Carsington DR C3 (18.44–27.60 m) covers the E_{2a3} and E_{2b1} bands which together correspond to an important transgression (Trewin and Holdsworth, 1973; Waters and Condon, 2012). The TOC_{pd} averages 3.5% (n = 27) and TOC_o 3.44% (n = 4). In both instances these values surpass the 2% limit set as a criterion for organic matter content that defines an unconventional play (Andrews, 2013; Gilman and Robinson, 2011; TNO, 2009). However, when the reactive, pyrolysable carbon content representing the generative part of the kerogen fraction is considered, no samples surpass the 2% boundary. Assigning AOM to a kerogen Type I is tentatively done by utilizing the autofluorescence properties of the kerogen fraction (Section 5.2). Kerogen Types II and III are better constrained by transmitted white light observations and average 62% and 1.8% respectively. This shows marine organic matter dominates over terrestrial organic matter which is significantly lower than the lower part of the section. The HI_o index averages 532 mg/g TOC_o and is well above the 250 mg/g TOC constraint (Charpentier and Cook, 2011; TNO, 2009) and falls in the 250–800 mg/g TOC interval suggested by Jarvie (2012). The siliceous mudstones contain variable amounts of carbonate (up to 24%) and one sample (SSK44595 at 22.99 m) has a low silica and carbonate content plotting in the ductile to brittle transition zone (Figure 8). No discrete smectite was identified in the sampled Carsington DR C3 interval, as required by Jarvie (2012) (Appendix 8). Both mineralogy and T_{max} values indicate however that the studied material is immature for gas generation (Section 5.3).

6.2 Karenight 1

The studied section of the Karenight 1 core covers the E_1 (Pendleian) to E_2 biozone transition (Figure 6). The lower part of the section (242.80–251.89 m) is dominated by mudstone with subordinate and interspersed limestone intervals. All samples of the lower part of Karenight 1 surpass 4% TOC with an average of 6.9%. When the pyrolysable carbon of TOC_{pd} is considered however, the average TOC_{pd} is 1.9% and only three samples pass the 2% threshold (Appendix 3). The organic matter mostly consists of heterogeneous AOM (80.5% on average) with an average calculated 17.4% of Type II (Table 4) and 1.3% Type III reflecting the very limited influx of terrestrially sourced AOM, also reflected in the low $\delta^{13}C_{OM}$ values. The HI_o reaches on average 554 mg/g TOC_o with TOC_o averaging 9.92%. These values fall in the prospectivity window described by Jarvie (2012). XRD analysis of the bottom part of Karenight 1 shows that the lithology varies from argillaceous to siliceous mudstones, but all samples have a silica content over 30% (Appendices 6 and 8).

The upper part of the Karenight 1 core (234.77–242.80 m) covers the E_2 biozone, possibly containing evidence of the E_{2b} Marine Band around 241.50 m. The TOC_{pd} values are less than in the lower part of the core (3.68%) and the kerogen fraction is composed of 78.6% heterogeneous AOM, a calculated average of 67% Type II kerogen (Table 4) and 2.7% Type III kerogen. Again, these values combined with the relatively light carbon isotopic signature show the dominance of marine conditions. The somewhat higher average values of Type III kerogen show the influence of terrestrial matter which is associated with the presence of siltstone intervals (Figure 6). The average calculated HI_o is somewhat lower than the bottom part of the section (500 mg/g TOC_o) while TOC_0 is significantly lower (4.69%). These values are still within the constraints of the prospectivity criteria (Table 1). The upper part of the section contains a highly variable amount of carbonates but all samples have a silicate content that surpasses the 30% threshold (Figure 8). No discrete smectite was identified in the sampled Karenight 1 interval (Appendix 8) as for Carsington DR C3, the mineralogy and T_{max} values indicate that the Karenight 1 material is immature for gas generation.

6.3 Implications for the prospectivity of Arnsbergian shales in the Southern part of the Pennine Basin

The Arnsbergian mudstones from the Morridge Formation in the Widmerpool and Edale Gulf proved by the Carsington DRC 3 and Karenight 1 boreholes were deposited coeval with active unconventional exploration targets in the Craven and Bowland Basins and the Upper Barnett Shales from the Fort Worth Basin (USA) (Figure 3). Karenight 1 contains more marine organic material and is characterized by higher FSI (Figure 5), TOC_{pd}, TOC_0 and HI_0 values than Carsington DR C3

(Tables 4 and 5), which exhibits frequent sandstone intervals and a higher fraction of kerogen Type III. The terrestrial material in the Morridge Formation originates from the Wales-Brabant High to the south of the Pennine Basin (Trewin and Holdsworth, 1973; Waters et al., 2009). Therefore, we hypothesise that when turbiditic flows entered the Pennine Basin sourced from the Wales-Brabant High to the south (Figure 1), most of the terrestrial material was deposited in the Widmerpool Gulf. The remnant of the south-eastern part of the Derbyshire High, located between Carsington DR C3 and Karenight 1 during the Arnsbergian represents a barrier to sediment input from the south into the Edale Gulf, resulting in the deposition of only a relatively small fraction of these sediments with a terrigenous character at Karenight 1. However, even in the intervals of Carsington DR C3 that are characterised by a terrestrial signature (e.g. 33.63–35 m and 40.5–44 m), marine influences are noticeable: Type II kerogen remains important in the palynofacies counts and $\delta^{13}C_{OM}$ exceeds -24‰. This suggests a continuous sedimentation of marine-derived material, punctuated by influxes of terrestrial material from the Wales-Brabant High diluting the marine deposits. This means that prospective intervals in both the Widmerpool and Edale Gulf are relatively thin (decimetre to metre scale) and consequently high resolution characterization of these intervals is required in future research to quantify reservoir fairways. Given the high diversity of spores recovered from both cores (Appendices 1 and 2), a comprehensive, quantitative re-evaluation of the spore biozonation from these intervals on a metre- to decimetre-scale (i.e., at a higher resolution than typical goniatite marine band cyclicity), may aid in the identification of the prospective intervals.

The work flow employed in the current study (Rock-Eval, stable isotope, XRD, epifluorescence, palynofacies analysis) gives a complete assessment of the organic matter of potentially prospective shale gas plays. This approach allows for a calculation of HI_o and TOC_o which give a more meaningful evaluation of prospecitivity estimates. In this way, we show that the most prospective part of the Carsington DRC3 borehole is the E_{2b1}–E_{2a3} with a HI_o of 465 mg/g TOC_o and TOC_o of 3.2% while for the Karenight 1 borehole the most prospective part is the E_1(?)–E_{2a} interval with an average HI_o of 504 mg/g TOC_o and TOC_o of 9.3%. In Table 5, these values are compared with the top 10 shale gas systems as reported by Jarvie (2012). The most prospective intervals of both the Carsington

DRC3 and the Karenight 1 boreholes have HI_o and TOC_o values that are comparable to the contemporaneous US shales. The least prospective intervals from the Carsington DRC3 core have values that are well below the contemporaneous US shales, most likely reflecting the higher amount of terrestrial material with on average 30.3% Type III kerogen. For the Barnett Shale, kerogen Type II with a minor admixture of Type III (Bruner and Smosna, 2011) has been reported. Though no actual palynofacies counts were cited, Jarvie et al. (2007) use a 95% Type II and 5% Type III for their calculation of HI_o for the Barnett Shale.

7. Conclusions

We investigated Namurian (late Mississippian) mudstones from two boreholes drilled in the southern part of the Pennine Basin (UK): the Carsington Dam Reconstruction C3 borehole from the Widmerpool Gulf and the Karenight 1 borehole from the Edale Gulf. Both prove mudstone-dominated intervals of Arnsbergian (Serpukhovian) age, with the Carsington DR C3 borehole comprising the E_{2b1}–E_{2a} marine bands, while the Karenight 1 borehole the E_{2b} and E_1 marine bands. We describe a fully integrated, multi-proxy approach to describe the geochemical, palynological and sedimentological properties:

Heterogeneous AOM dominates the E_{2b1}–E_{2a3} samples in the Carsington core with important contributions of Type II kerogen and only minor amounts of Type III kerogen. The E_{2a} interval below E_{2a3} contains markedly less heterogeneous AOM and a more important Type III kerogen fraction. The highest TOC_{pd} values are reported from the E_{2b1}–E_{2a3} interval (3.52% on average). However, when the pyrolysable content of the Rock-Eval™ analyses is considered, none of the TOC_{pd} of the Carsington samples exceeds 2%. The calculated HI_o and TOC_o for E_{2b1}–E_{2a3} averages respectively 465 mg/g TOC_o and 3.2%. For E_{2a} below E_{2a3}, HI_o averages 396 mg/g TOC and TOC_o 1.0%. Carsington DR C3 contains mainly siliceous mudstones with a variable carbonate content (E_{2b1}–E_{2a3}) and argillaceous mudstones with a very low carbonate content (E_{2a} below E_{2a3}). The bottom part of the section is further characterized by two sandstone intervals interpreted as turbidites entering the Widmerpool Gulf from the Wales Brabant High. Based on the criteria for prospective shale gas plays, Carsington DR C3 has reasonably high organic contents and hydrogen indices. Calculated HI_o and TOC_o are within the limits of known producing plays (Tables 1 and 5). However, the XRD results and T_{max} values suggest the Namurian deposits of the Widmerpool Gulf are too immature for gas generation.

The Karenight 1 core samples are dominated by heterogeneous AOM throughout while Kerogen Type II is also important and Type III kerogen is of minor importance. TOC_{pd} surpasses 2% in 68 of 72 considered samples, however when the pyrolysable carbon content is considered, only 3 samples surpass 2%. In the bottom part of Karenight 1 (242.80–251.89 m) HI_o averages 504 mg/g TOC_o with a TOC_o of 9.3% while in the top part (234.77–242.80 m) HI_o averages 448 mg/g TOC with a TOC_o of 4.4%. In the Karenight 1 core we find carbonate poor siliceous and argillaceous mudstones in the bottom part and mudstones with a markedly higher carbonate content in the top part. The clearest marine intervals (lowest $\delta^{13}C_{OM}$ combined with high TOC_{pd}) occur in the lower part of Karenight 1 yielding some of the most organic rich Namurian deposits in the Pennine Basin. As for the Namurian deposits in the Widmerpool Gulf, the Namurian strata in the Edale Gulf have organic contents combined with hydrogen indices that fall well within the limits of known shale gas plays, but T_{max} suggests the deposits are immature for gas.

The terrestrial material that enters the southern Pennine Basin likely originates from the Wales Brabant High and therefore we conclude that most of the terrestrial material was deposited in the Widmerpool Gulf as turbidite flows and only a relatively small fraction reached the Edale Gulf, resulting in a more marine character in the Karenight 1 core. However, there is still a considerable amount of kerogen Type II in Carsington DR C3, even in intervals with a terrigenous sedimentary signature. This points to continuous marine conditions across the southern part of the Pennine Basin, at times diluted by turbiditic deposits, most likely related to. Because of this, the intervals prospective for hydrocarbon generation in especially the Widmerpool Gulf and to a lesser extent in the Edale Gulf, are relatively thin (decimetre to meter scale). Consequently, high resolution characterization, at sub-marine band resolution, of these intervals should be the focus of future research. Quantitative spore analysis and fluorescence microscopy may be of considerable help to achieve this goal given the high diversity of well-preserved spores recovered in the current study.

Acknowledgements

All authors publish with the approval of the Executive Director of the British Geological Survey. Jane Flint is thanked for the preparation of the palynological slides. Ian Mounteney is acknowledged for his assistance with the XRD analyses and Chris Kendrick for the stable isotope analyses. The staff of the British Geological Core Store, Keyworth, are thanked for their help in accessing cores and facilitating sample collection. We would also like to thank reviewers Hugh Daigle and Patrick J. Dowey and Associate Editor Hui Tian for their comments and suggestions on an earlier draft of this work.

References

Aitkenhead, N., 1991. Carsington Dam Reconstruction: notes on the stratigraphy and correlation of groundwater monitoring, British Geological Survey Technical Report GA/90F/58, 22 pp.

Aitkenhead, N., Barclay, W.J., Brandon, A., Chadwick, R., Chisholm, J.I., Cooper, A.H. and Johnson, E.W., 2002. British regional geology: the Pennines and adjacent areas. British Geological Survey, Nottingham, UK, 206 pp.

Anderson, T., 2014. Key Parameters for Liquid-Rich Unconventional Plays: Case Studies from North America. AAPG Search and Discovery Article 80354, 33.

Andrews, I.J., 2013. The Carboniferous Bowland Shale gas study: geology and resource estimation. British Geological Survey for the Department of Energy and Climate Change, London, UK, 64 pp. https://www.gov.uk/government/uploads/system/uploads/attachment_data/file/226874/BGS_DECC_BowlandShaleGasReport_MAIN_REPORT.pdf.

Berner, R.A., Petsch, S.T., Lake, J.A., Beerling, D.J., Popp, B.N., Lane, R.S., Laws, E.A., Westley, M.B., Cassar, N., Woodward, F.I., 2000. Isotope fractionation and atmospheric oxygen: implications for Phanerozoic O2 evolution. Science 287, 1630–1633. http://dx.doi.org/10.1126/science.287.5458.1630.

Bisat, W.S., 1923. The Carboniferous Goniatites of the North of England and their Zones. Proc. Yorkshire Geol. Soc. 20, 40–124. http://dx.doi.org/10.1144/pygs.20.1.40.

Blackwell, J., 2013. The story of Heathfield's natural gas find. Sussex Industrial History 43, 11–19.

Bruner, K.R., Smosna, R., 2011. A comparative study of the Mississippian Barnett Shale, Fort Worth Basin, and Devonian Marcellus Shale, Appalachian Basin. US Department of Energy, pp. 118.

Charpentier, R.R., Cook, T.A., 2011. USGS Methodology for assessing continuous petroleum resources. US Geological Survey Open-File Report, 2011-1167, 75pp.

Cleal, C.J., Thomas, B.A., 2005. Palaeozoic tropical rainforests and their effect on global climates: is the past the key to the present? Geobiology 3, 13–31. http://dx.doi.org/10.1111/j.1472-4669.2005.00043.x.

Combaz, A., 1980. Les kérogènes vus au microscope, in: Durand, B. (Ed.), Kerogen. Insoluble organic matter from sedimentary rocks. Éditions Technip, Paris, France, pp. 55–111.

Cooper, B. S. and Barnard, P.C., 1984. Source rock and oils of the central and northern North Sea, in: Demaison, G., Murris, R. J. (Eds.) Petroleum Geochemistry and Basin Evalutaion, AAPG mem., 35, pp. 303–314.

Craig, H., 1953. The geochemistry of the stable carbon isotopes. Geochim. Cosmochim. Acta 3, 53–92. http://dx.doi.org/10.1016/0016-7037(53)90001-5.

Cuss, R.J., Wiseall, A.C., Hennissen, J.A.I., Waters, C.N., Kemp, S.J., Ougier-Simonin, A., Holyoake, S., Haslam, R.B., 2015. M4ShaleGas-Measuring, monitoring, mitigating managing the environmental impact of shale gas - Review of hydraulic fracturing state-of-the-art report for the M4ShaleGas, Keyworth, Nottingham, UK, 82 pp.

Davydov, V.I., Korn, D., Schmitz, M.D., Gradstein, F.M., Hammer, O., 2012. Chapter 23 - The Carboniferous Period, in: Gradstein, F.M., Ogg, J.G., Schmitz, M.D., Ogg, G.M. (Eds.), The Geologic Time Scale. Elsevier, Boston, pp. 603–651. http://dx.doi.org/10.1016/B978-0-444-59425-9.00023-8.

Drewery, S., Cliff, R.A., Leeder, M.R., 1987. Provenance of Carboniferous sandstones from U-Pb dating of detrital zircons. Nature 325, 50–53. http://dx.doi.org/10.1038/325050a0.

Ewbank, G., Manning, D.A.C., Abbott, G.D., 1993. An organic geochemical study of bitumens and their potential source rocks from the South Pennine Orefield, Central England. Org. Geochem. 20, 579–598. http://dx.doi.org/10.1016/0146-6380(93)90025-7.

Fraser, A.J., Gawthorpe, R.L., 1990. Tectono-stratigraphic development and hydrocarbon habitat of the Carboniferous in northern England. Geological Society, London, Special Publications 55, 49–86. http://dx.doi.org/10.1144/gsl.sp.1990.055.01.03.

Gawthorpe, R.L., 1987. Tectono-sedimentary evolution of the Bowland Basin, N England, during the Dinantian. J. Geol. Soc. 144, 59–71. http://dx.doi.org/10.1144/gsjgs.144.1.0059.

Gilman, J., Robinson, C., 2011. Success and Failure in Shale Gas Exploration and Development: Attributes that Make the Difference, AAPG International Conference and Exhibition. American Association for Petroleum Geologists, Calgary, Alberta, Canada, 31 pp.

Gross, D., Sachsenhofer, R.F., Bechtel, A., Pytlak, L., Rupprecht, B., Wegerer, E., 2014. Organic geochemistry of Mississippian shales (Bowland Shale Formation) in central Britain: Implications for depositional environment, source rock and gas shale potential. Mar. Pet. Geol. 59, 1–21. http://dx.doi.org/10.1016/j.marpetgeo.2014.07.022.

Gutteridge, P., 1991. Aspects of dinantian sedimentation in the Edale Basin, North Derbyshire. Geol. J. 26, 245–269. http://dx.doi.org/10.1002/gj.3350260305.

Horsfield, B., 1984. Pyrolysis studies and petroleum exploration, in: Brooks, J., Welte D. (Eds.), Advances in Petroleum Geochemistry, pp. 247–298.

Holdsworth, B.K., Collinson, J.D., 1988. Millstone Grit cyclicity revisited, in: Besly, B.M., Kelling, G. (Eds.), Sedimentation in a synorogenic basin complex. Blackie, Glasgow, UK, pp. 132–152.

Holliday, D.W., Molyneux, S.G., 2006. Editorial statement: new official names for the subsystems, series and stages of the Carboniferous System – some guidance for contributors to the *Proceedings*. Proc. Yorkshire Geol. Soc. 56, 57–58. http://dx.doi.org/10.1144/pygs.56.1.57.

Isbell, J.L., Miller, M.F., Wolfe, K.L., Lenaker, P.A., 2003. Timing of Paleozoic glaciation in Gondwana: was glaciation responsible for the development of Northern Hemisphere cyclothems?. Geol. S. Am. S., 370, 5–24.

Jarvie, D.M., 2012. Shale resource systems for oil and gas: Part 1—Shale-gas resource systems, in: Breyer, J.A. (Ed.), Shale reservoirs—Giant resources for the 21st century:. American Association of Petroleum Geologists, Tulsa, Oklahoma, pp. 69–87. http://dx.doi.org/10.1306/13321477M973494.

Jarvie, D.M., 2015. Geochemical assessment of unconventional shale gas resource systems, in: Rezaee, R. (Ed.), Fundamentals of Gas Shale Reservoirs. John Wiley & Sons, Hoboken, NJ, pp. 47–69.

Jarvie, D.M., Hill, R.J., Ruble, T.E., Pollastro, R.M., 2007. Unconventional shale-gas systems: The Mississippian Barnett Shale of north-central Texas as one model for thermogenic shale-gas assessment. AAPG Bull. 91, 475–499. http://dx.doi.org/10.1306/12190606068.

Kemp, S.J., Ellis, M.A., Mounteney, I. and Kender, S. 2016. Palaeoclimatic implications of high-resolution clay mineral assemblages preceding and across the onset of the Palaeocene–Eocene Thermal Maximum, North Sea Basin. Clay Minerals, 51(5), 793–813. http://dx.doi.org/10.1180/claymin.2016.051.5.08.

Könitzer, S.F., Davies, S.J., Stephenson, M.H., Leng, M.J., 2014. Depositional Controls On Mudstone Lithofacies In A Basinal Setting: Implications for the Delivery of Sedimentary Organic Matter. J. Sediment. Res. 84, 198–214. http://dx.doi.org/10.2110/jsr.2014.18.

Kump, L.R., Brantley, S.L., Arthur, M.A., 2000. Chemical Weathering, Atmospheric CO_2, and Climate. Annu. Rev. Earth Planet. Sci. Lett. 28, 611–667. http://dx.doi.org/10.1146/annurev.earth.28.1.611.

Lee, A.G., 1988. Carboniferous basin configuration of central and northern England modelled using gravity data, in: Besly, B.M., Kelling, G. (Eds.), Sedimentation in a synorogenic basin complex. Blackie, Glasgow, UK, pp. 69–84.

Leeder, M.R., 1982. Upper Palaeozoic basins of the British Isles—Caledonide inheritance versus Hercynian plate margin processes. J. Geol. Soc. 139, 479–491. http://dx.doi.org/10.1144/gsjgs.139.4.0479.

Leeder, M.R., McMahon, A.H., 1988. Tests and consequences of the extensional theory for Carboniferous basin evolution in Northern England, in: Besly, B.M., Kelling, G. (Eds.), Sedimentation in a Synorogenic Basin Complex: the Upper Carboniferous of Northwest Europe. Blackie, Glasgow and London, pp. 43–52.

Lewan, M.D., 1986. Stable carbon isotopes of amorphous kerogens from Phanerozoic sedimentary rocks. Geochim. Cosmochim. Acta 50, 1583–1591. http://dx.doi.org/10.1016/0016-7037(86)90121-3.

Lewis, R., Ingraham, D., Pearcy, M., Williamson, J., Sawyer, W., Frantz, J., 2004. New Evaluation Techniques for Gas Shale Reservoirs, Schlumberger Reservoir Symposium 2004, Houston, Texas.

Lin, R., Davis, A., 1988. The chemistry of coal maceral fluorescence: with special reference to the Huminite/Vitrinite Group. Special Research Report, Energy and Fuels Research Center, Pennsylvania State University, 306 pp.

Loucks, R.G., Ruppel, S.C., 2007. Mississippian Barnett Shale: Lithofacies and depositional setting of a deep-water shale-gas succession in the Fort Worth Basin, Texas. AAPG Bull. 91, 579–601. http://dx.doi.org/10.1306/11020606059.

Martinsen, O.J., Collinson, J.D., Holdsworth, B.K., 1995. Millstone Grit Cyclicity Revisited, II: Sequence Stratigraphy and Sedimentary Responses to Changes of Relative Sea-Level, Sedimentary Facies Analysis. Blackwell Publishing Ltd., pp. 305–327. http://dx.doi.org/10.1002/9781444304091.ch13.

Maynard, J.B., 1981. Carbon isotopes as indicators of dispersal patterns in Devonian-Mississippian shales of the Appalachian Basin. Geology 9, 262–265. http://dx.doi.org/10.1130/0091-7613(1981)9<262:ciaiod>2.0.co;2.

Maynard, J.R., Leeder, M.R., 1992. On the periodicity and magnitude of Late Carboniferous glacio-eustatie sea-level changes. J. Geol. Soc. 149, 303–311. http://dx.doi.org/10.1144/gsjgs.149.3.0303.

McKerrow, W.S., Scotese, C.R., 1990. Palaeozoic palaeogeography and biogeography. Geological Society, London, UK, 435 pp.

Merriman, R.J. and Kemp, S.J. 1996. Clay minerals and sedimentary basin maturity. Mineralogical Society Bulletin, 111, 7–8.

Montgomery, S.L., Jarvie, D.M., Bowker, K.A., Pollastro, R.M., 2005. Mississippian Barnett Shale, Fort Worth basin, north-central Texas: Gas-shale play with multi-trillion cubic foot potential. AAPG Bull. 89, 155–175. http://dx.doi.org/10.1306/09170404042.

Newell, A.J., Vane, C.H., Sorensen, J.P.R., Moss-Hayes, V., Gooddy, D.C., 2016. Long-term Holocene groundwater fluctuations in a chalk catchment: evidence from Rock-Eval pyrolysis of riparian peats. Hydrol. Processes 30, 4556-4567. http://dx.doi.org/4556-4567 10.1002/hyp.10903.

Newman, J.W., Parker, P.L., Behrens, E.W., 1973. Organic carbon isotope ratios in Quaternary cores from the Gulf of Mexico. Geochim. Cosmochim. Acta 37, 225–238. http://dx.doi.org/10.1016/0016-7037(73)90130-0.

Passey, Q.R., Creaney, S., Kulla, J.B., Moretti, F.J., Stroud, J.D., 1990. A practical model for organic richness from porosity and resistivity logs. AAPG Bull. 74, 1777–1794.

Peters-Kottig, W., Strauss, H., Kerp, H., 2006. The land plant $\delta^{13}C$ record and plant evolution in the Late Palaeozoic. Palaeogeog. Palaeoclimatol. Palaeoecol. 240, 237–252. http://dx.doi.org/10.1016/j.palaeo.2006.03.051.

Phillips, T.L., diMichele, W.A., 1990. Comparative Ecology and Life-History Biology of Arborescent Lycopsids in Late Carboniferous Swamps of Euramerica. Annals of the Missouri Botanical Garden 79, 560–588. http://dx.doi.org/10.2307/2399753.

Pollastro, R.M., 2003. Geologic and Production Characteristics Utilized in Assessing the Barnett Shale Continuous (Unconventional) Gas Accumulation, Barnett-Paleozoic Total Petroleum System, Fort Worth Basin, Texas, Barnett Shale Symposium, Ellison Miles Geotechnology Institute at Brookhaven College, Dallas, Texas, 6pp.

Pollastro, R.M., Hill, R.J., Jarvie, D.M., Mitchell, H.E., 2003. Assessing Undiscovered Resources of the Barnett-Paleozoic Total Petroleum System, Bend Arch–Fort Worth Basin Province, Texas. AAPG Search and Discovery Article, 17.

Pollastro, R.M., Jarvie, D.M., Hill, R.J., Adams, C.W., 2007. Geologic framework of the Mississippian Barnett Shale, Barnett-Paleozoic total petroleum system, Bend arch–Fort Worth Basin, Texas. AAPG Bull. 91, 405–436. http://dx.doi.org/10.1306/10300606008.

Posamentier, H.W., Jervey, M.T., Vail, P.R., 1988. Eustatic controls on clastic deposition I - conceptual framework, in: Wilgus, C.K., Hastings, B.S., Kendall, C.G.S., Posamentier, H.W., Ross, C.A., Van Wagoner, J.C. (Eds.), Sea-level Changes: an Integrated Approach. Special Publications Society of Economic Paleontologists and Mineralogists, Tulsa, USA, pp. 109–124.

Ramsbottom, W.H.C., 1977. Major Cycles of Transgression and Regression (Mesothems) in the Namurian. Proc. Yorkshire Geol. Soc. 41, 261–291. http://dx.doi.org/10.1144/pygs.41.3.261.

Ramsbottom, W.H.C., 1979. Rates of transgression and regression in the Carboniferous of NW Europe. J. Geol. Soc. 136, 147–153. http://dx.doi.org/10.1144/gsjgs.136.2.0147.

Ramsbottom, W.H.C., Rhys, G.H., Smith, E.G., Bullerwell, W., Cosgrove, M.E., Elliot, R.W., 1962. Boreholes in the Carboniferous rocks of the Ashover district, Derbyshire. Bulletin of the Geological Survey of Great Britain, 19, 75–168.

Riegel, W., 2008. The Late Palaeozoic phytoplankton blackout — Artefact or evidence of global change? Rev. Palaeobot. Palyno. 148, 73–90 http://dx.doi.org/10.1016/j.revpalbo.2006.12.006.

Robert, P., 1988. Organic metamorphism and geothermal history : microscopic study of organic matter and thermal evolution of sedimentary basins. Kluwer, Dordrecht, The Netherlands, 311 pp.

Robinson, J.M., 1990. The burial of organic carbon as affected by the evolution of land plants. Hist. Biol. 3, 189–201 http://dx.doi.org/10.1080/08912969009386521.

Selley, R.C., 1987. British shale gas potential scrutinized. Oil Gas J. 15, 62–64.

Selley, R.C., 2012. UK shale gas: The story so far. Mar. Pet. Geol. 31, 100–109 http://dx.doi.org/10.1016/j.marpetgeo.2011.08.017.

Silverman, S.R., Epstein , S., 1958. Carbon isotopic compositions of petroleums and other sedimentary organic materials. AAPG Bull. 42, 998–1012.

Skempton, A.W., Vaughan, P.R., 1993. The failure of Carsington Dam. Géotechnique 43, 151–173 http://dx.doi.org/10.1680/geot.1993.43.1.151.

Słowakiewicz, M., Tucker, M.E., Vane, C.H., Harding, R., Collins, A., Pancost, R.D., 2015. Shale-gas potential of the mid-Carboniferous Bowland-Hodder unit in the Cleveland basin (Yorkshire), Central Britain. J. Pet. Geol 38, 59–75. http://dx.doi.org/10.1111/jpg.12598.

Smith, N., Turner, P., Williams, G., 2010. UK data and analysis for shale gas prospectivity. Petroleum Geology Conference Series 7, 1087–1098.

Snyder, R. L., Bish, D. L., 1989. Quantitative analysis, in: Bish, D. J., Post, J. E. (Eds.) Modern Powder Diffraction, Reviews in Mineralogy, 20, Mineralogical Society of America, Washington DC, pp. 101–144.

Sone, H., Zoback, M.D., 2013. Mechanical properties of shale-gas reservoir rocks — Part 1: Static and dynamic elastic properties and anisotropy. Geophysics 78, D381–D392 http://dx.doi.org/10.1190/geo2013-0050.1.

Stephenson, M.H., Angiolini, L., Cozar, P., Jadoul, F., Leng, M.J., Millward, D., Chenery, S., 2010. Northern England Serpukhovian (early Namurian) farfield responses to southern hemisphere glaciation. J. Geol. Soc. 167, 1171–1184. http://dx.doi.org/10.1144/0016-76492010-048.

Stephenson, M.H., Millward, D., Leng, M.J., Vane, C.H., 2008. Palaeoecological and possible evolutionary effects of early Namurian (Serpukhovian, Carboniferous) glacioeustatic cyclicity. J. Geol. Soc. 165, 993–1005 http://dx.doi.org/10.1144/0016-76492007-153.

Stevenson, I.P., Gaunt, G.D., Calver, M.A., Harrison, R.K., Mitchell, M., Ramsbottom, W.H.C., 1971. Geology of the country around Chapel en le Frith. Explanation of sheet 99, Memoir of the Geological Survey of Great Britain. HMSO, London, UK, 510 pp.

Steward, D.B., 2007. The Barnett Shale play: Phoenix of the Fort Worth Basin - a history. The Fort Worth Geological Society, Dallas, Texas, 202 pp.

Sub-Wealden Exploration Company, T., 1873. Sub-Wealden Exploration. Nature 7, 288. http://dx.doi.org/10.1038/007288a0.

Thomas, B.A., 1978. Carboniferous lepidodendraceae and lepidocarpaceae. The Botanical Review 44, 321–364. http://dx.doi.org/10.1007/bf02957853.

TNO, 2009. Inventory non-conventional gas. TNO Built environment and Geosciences, Utrecht, 188 pp.

Topley, W., Godwin-Austen, R., Willett, H., 1872. The British Association Section C. - Geology. Nature 6, 361 http://dx.doi.org/10.1038/006357a0.

Trewin, N.H., Holdsworth, B.K., 1973. Sedmimentation in the lower Namurian rocks of the North Staffordshire Basin. Proc. Yorkshire Geol. Soc. 39, 371–408

Tyson, R.V., 1995. Sedimentary Organic Matter, Chapman & Hall, London, 648 pp.

Tyson, R.V., 2006. Calibration of hydrogen indices with microscopy: A review, reanalysis and new results using the fluorescence scale. Org. Geochem. 37, 45–63. http://dx.doi.org/10.1016/j.orggeochem.2005.08.018.

U.S.Energy Information Administration, 2011. Review of Emerging Resources: U.S. Shale Gas and Shale Oil Plays, US Energy Information Administration, Washington DC, 105 pp.

Van Gijzel, P., 1982. Characterization and identification of kerogen and bitumen and determination of thermal maturation by means of qualitative and quantitative microscopical techniques. Soc. Econ. Pa., Short Course, 159–216.

Veevers, J.J., Powell, C.M., 1987. Late Paleozoic glacial episodes in Gondwanaland reflected in transgressive-regressive depositional sequences in Euramerica. GSA Bulletin 98, 475–487. http://dx.doi.org/10.1130/0016-7606(1987)98<475:LPGEIG>2.0.CO;2.

Walper, J.L., 1982. Plate Tectonic Evolution of the Fort Worth Basin, in: Martin, C.A. (Ed.), Petroleum Geology of the Fort Worth Basin and Bend Arch Area. Dallas Geological Society, Dallas, Texas, pp. 237–251.

Waters, C.N., Browne, M.A.E., Dean, M.T., Powell, J.H., 2007. Lithostratigraphical framework for Carboniferous successions of Great Britain (Onshore). British Geological Survey Research Report, RR/07/01, 70 pp.

Waters, C.N., Condon, D.J., 2012. Nature and timing of Late Mississippian to Mid-Pennsylvanian glacio-eustatic sea-level changes of the Pennine Basin, UK. J. Geol. Soc. 169, 37–51 http://dx.doi.org/10.1144/0016-76492011-047.

Waters, C.N., Waters, R.A., Barclay, W.J., Davies, J.R., 2009. A lithostratigraphical framework for the Carboniferous successions of southern Great Britain (onshore), British Geological Survey Research Report, RR/09/01, 194 pp.

Wilson, A.A., Stevenson, I.P., 1973. Karenight No. 1, Institute of Geological Sciences Record of Shaft or Borehole. British Geological Survey, Keyworth, Nottingham, U.K., 14 pp.

Table captions

Table 1: Evaluation of widely accepted criteria to assess the prospectivity of shale gas plays.

Table 2: Kerogen typing applied in the current study based on Tyson (1995).

Table 3: Present day Rock-Eval parameters and HI_o and TOC_o for Carsington DR C3 based on the calculated kerogen typing using a combination of palynofacies analysis and the fluorescence scale.

Table 4: Present day Rock-Eval parameters and HI_o and TOC_o for Karenight 1 based on the calculated kerogen typing using a combination of palynofacies analysis and the fluorescence scale.

Table 5: Comparison of the results of the current study with the top 10 shale gas plays in the US (Jarvie, 2012).

Figure Captions

Figure 1: Mississippian paleogeography of Southern Britain, showing major basin bounding faults and the location of the Carsington Dam Reconstruction C3 and Karenight 1 boreholes (based on Waters et al., 2009). BH = Bowland High; BT = Bowland Trough; CLH = Central Lancashire High; DH = Derbyshire High; EG = Edale Gulf; GT = Gainsborough Trough; LDH = Lake District High; Manx High; WG = Widmerpool Gulf. Contains Ordnance Survey data © Crown Copyright and database rights 2017.

Figure 2: A: Map of the U.K. with the study area highlighted in green; B: Location of the Carsington Dam Reconstruction C3 (yellow) and Karenight 1 (red) Boreholes in relation to bedrock geology. U. = Upper; M. = Middle; L. = Lower. Digital geological map data BGS © NERC; contains Ordnance Survey data © Crown Copyright and database rights 2017.

Figure 3: Generalized stratigraphic column for the Carboniferous in the Pennine Basin (U.K.) with the Morridge Formation highlighted and correlation with the Fort Worth Basin (U.S.). Global chronostratigraphy and North American Stages follow Davydov et al.(2012), regional chronostratigrphy for European and UK (sub)stages follow Holliday and Molyneux (2007), the lithostratigraphy for the Fort Worth Basin is based on Pollastro et al. (2003; 2007) and the lithostratigraphy of the UK basins follows the framework of Waters et al. (2007). obs. = obsolete; Rotlieg. = Rotliegend; Steph. = Stephanian; Duckmant. = Duckmantian; Langs. = Langsettian; Yead. = Yeadonian; Mars. = Marsdenian; Kinder. = Kinderscoutian; Chokie. = Chokierian; Pendl. = Pendleian; Arund. = Arundian; Chad. = Chadian; Caddo Cr. = Caddo Creek; Gr. = Group; Sm. = Smithwick; Fm. = Formation; PLCM = Pennine Lower Coal Measures Formation; Ross. = Rossendale; Mars. = Marsden Formation.

Figure 4: Legend for the lithostratigraphy of the Carsington Reconstruction DRC3 and Karenight boreholes Figures 5 and 6.

Figure 5: Lithostratigraphical, geochemical and palynological results of the Carsington DRC3 (17.50–55.50 m). The legend for the lithological column is displayed in Figure 4. The Western European marine band classification follows Aitkenhead (1991). Legend detailed in Figure 4.

Figure 6: Lithostratigraphical, geochemical and palynological results of the Karenight 1 Borehole (234.7–251.9 m). The legend for the lithological column is displayed in Figure 4. The tentative Western European marine band classification follows Wilson and Stevenson (1973). Legend detailed in Figure 4.

Figure 7: Ternary Phytoclast-AOM-Palynomorphs plot (modified after Tyson, 1995) for the samples from the Carsington Dam Reconstruction C3 core (black) and the Karenight 1 core (red).

Figure 8: Ternary carbonates-clay-silicates summarizing the XRD results from the Carsington Dam Reconstruction C3 (black) and Karenight 1 (red) cores compared to Palaeozoic shale plays in the US (yellow; Anderson, 2014).

Figure 9: Total organic carbon (TOC) model from deposition to analysis. Subscripts ‘o’ and ‘pd’ indicate original and present day estimates respectively. The parameters generative organic carbon (GOC) and non-generative organic carbon (NGOC) are defined following Jarvie (2012) and Jarvie (2015). HC = hydrocarbons; PC = Pyrolysed Carbon.

Figure 10: Organic matter $\delta^{13}C$ versus TOC_{pd} values for Carsington DRC3 (black) and Karenight 1 (red) samples.

Plate I: Main palynofacies constituents in the Arnsbergian shales of the Widmerpool and Edale Gulf. 1: AOM with a gelified matrix (SSK46366 slide 1; EF: Q30/4); 2: Magnification of 1 (white rectangle) on fambroidal (white arrows) and euhedral (yellow arrows) pyrite; 3 Heterogeneous, grumose AOM (SSK45595 slide 1; EF: O19/4); 4 Imprints of framboidal pyrite (yellow arrows) on a fragment of Pellicular AOM (SSK4639 slide 1; EF: U21 2); 5 Black phytoclast (black arrow) attached to a fragment of Vitrinite *sensu* Combaz (1980) (SSK45594 slide 1, EF: Q7/40; 6 *Botryococcus* spp. (SSK45594 slide 1; p20/2).

Plate II: Most common miospores encountered in the Arnsbergian shales of the Widmerpool and Edale Gulf. Scale bars indicate 10 µm. 1: *Lycospora pusilla* (SSK45628 slide 1; England Finder coordinates (EF): P28/3); 2: *Cingulizonates bialatus* (SSK45628 slide 4; EF: J58/2); 3: *Granulatisporites granulatus* (SSK45636 slide 1; EF: O27/0); 4: *Savitrisporites nux* (SSK46301 slide 3; EF: P22/1); 5: *Densosporites anulatus* (SSK45636 slide 1; EF: P26/1); 6: *Crassispora kosankei* (SSK46331 slide 1; EF: H30/1).

Criterion	Definitions	Carsington DRC3 (Widmerpool Gulf)	Karenight 1 (Edale Gulf)
Organic matter content (TOC_{pd})	>2 % (TNO, 2009; Gilman and Robinson, 2011; Andrews, 2013) >4 % (Lewis et al., 2004)	142 of 169 samples have a TOC_{pd} >1%; 97 samples have a TOC_{pd} >2%. E_{2a3}–E_{2b1}: highest TOC_{pd} averaging 3.52%. When PC is considered, no samples exceed the 2% threshold.	71 of 72 samples have a TOC_{pd} >1; 68 have TOC_{pd} >2. When PC is considered, 38 samples surpass 1%; 3 samples exceed 2%.
Kerogen Type	Type I, II, IIS (Charpentier and Cook, 2011) Type II (Jarvie 2012)	With fluorescence weighting of heterogeneous AOM: E_{2b1}–E_{2a3} (18.02–27.32 m): Type I: 34.3 %; Type II: 40.3 %; Type III: 22.2 %; Type IV: 0.8 %. E_{2a} below E_{2a3} (27.32– 55.46 m): Type I: 19.8 %; Type II: 46.9 %; Type III: 30.3 %; Type IV: 1.3 %.	With fluorescence weighting of heterogeneous AOM: E_{2b}(?) and above (234.77–242.80 m): Type I: 26.1%; Type II: 51.3%; Type III: 18.3%; Type IV: 0.2%. E_{2a}–E_1 (242.80–251.89 m): Type I: 40.1%; Type II: 40.0%; Type III: 16.5%; Type IV: 0.7%.
Original Hydrogen index (HI_o) and original TOC (TOC_o)	>250 mg/g (TNO, 2009; Charpentier and Cook 2011) 250–800 mg/g (Jarvie, 2012)	E_{2b1}–E_{2a3} (18.02–27.32 m): HI_o averages 465 mg/g TOC_o; TOC_o averages 3.2%. E_{2a} below E_{2a3} (27.32– 55.46 m): HI_o averages 396 mg/g TOC_o; TOC_o averages 1.0%.	E_{2b}(?) and above (234.77–242.80 m): HI_o averages 448 mg/g TOC_o; TOC_o averages 4.4 %. E_{2a}–E_1 (242.80–251.89 m): HI_o averages 504 mg/g; TOC_0 averages 9.3 %.
Mineralogy and clay content	Low clay content (<35%) (Andrews, 2013). Significant silica content (>30%) with some carbonate and presence of non-swelling clays (Jarvie, 2012). Ductile brittle transition zone 40-60% clay content.	E_{2b1}–E_{2a3} (18.02–27.32 m): dominantly siliceous mudstones with a variable carbonate content (maximum 24%); clay content: 10–54%. E_{2a} below E_{2a3} (27.32– 55.46 m): dominantly argillaceous mudstones with a very low carbonate content (maximum 2%); clay content: 11–78%.	E_{2b}(?) and above (234.77–242.80 m): siliceous–argillaceous mudstones with varying amounts of carbonates (maximum 49%); clay content: 27–59%. E_{2a}–E_1 (242.80–251.89 m): siliceous–argillaceous mudstones with a low carbonate content (maximum 10%); clay content: 34–62%.

Table 1

Kerogen type	Organic constituent
Type I	Algal material
Type II	Spores and pollen, phytoplankton, cuticles
Type III	Homogeneous AOM, phytoclasts
Type IV	Coalified material

Table 2

European Substage	Goniatite Biozone	W. European Marine Band	BGS Sample	Depth (m)	HI_{pd} (mg/g TOC_{pd})	HI_o (mg/g TOC_o)	TOC_{pd} (%)	TOC_{pdNGOC} (%)	TOC_o (%)	ΔTOC (TOC_{pdNGOC}− TOC_o) (%)	FSI	Type I	Type II	Type III	Type IV
Arnsbergian	E_{2b}	E_{2b1}	SSK45587	18.44	256	435	3.63	2.78	3.86	1.43	2.46	27.9	42.4	28.7	0.7
	E_{2a} *Cravenoceras cowlingense*	E_{2a3}	SSK45595	22.99	153	486	2.47	2.13	2.97	1.23	2.58	34.9	46.1	13.0	1.3
			SSK45604	25.40	293	454	3.45	2.54	3.55	1.37	2.91	34.8	35.8	26.0	1.0
			SSK45607	26.18	313	487	2.53	1.81	2.42	1.00	3.13	39.5	36.8	21.0	0.0
			SSK45616	28.22	172	276	1.23	1.02	1.04	0.25	1.32	9.1	32.5	51.0	0.3
			SSK45621	28.94	177	529	2.12	1.79	2.49	1.12	2.74	38.8	50.5	8.0	1.7
			SSK45628	30.20	80	450	1.63	1.52	1.87	0.71	2.26	25.2	52.2	21.7	0.3
			SSK45632	30.89	211	419	0.84	0.66	0.51	0.18	2.13	23.6	46.4	27.3	0.0
			SSK45634	31.11	66	266	0.29	0.27	0.08	0.02	1.00	6.2	33.5	55.7	4.0
			SSK45636	31.61	119	387	2.06	1.84	2.28	0.75	1.98	19.1	46.7	28.2	0.0
			SSK45647	33.63	58	356	1.45	1.37	1.55	0.47	1.24	11.2	51.1	33.3	2.7
			SSK46019	37.10	147	460	3.67	3.18	4.62	1.80	1.69	22.8	60.2	14.7	1.0
			SSK46032	39.55	331	530	2.13	1.51	1.98	0.89	2.73	38.0	52.0	8.3	1.0
			SSK46301	40.83	119	292	1.82	1.62	1.85	0.46	0.86	4.9	44.1	45.7	4.7
			SSK46311	42.58	152	265	3.42	2.88	3.44	0.77	1.14	6.9	31.5	58.3	3.0
			SSK46316	43.26	147	408	0.51	0.44	0.18	0.06	2.06	22.1	45.9	29.3	0.7
			SSK46331	46.08	299	539	2.29	1.70	2.33	1.07	2.75	39.3	52.0	7.7	1.0
			SSK46340	48.75	100	462	3.02	2.75	3.92	1.54	2.33	27.7	51.0	20.7	0.0
			SSK46348	50.46	220	424	2.55	2.06	2.69	0.97	2.17	21.6	52.0	22.7	0.3
			SSK46351	51.86	229	430	2.55	2.04	2.67	0.98	1.53	16.0	63.7	19.3	0.3
			SSK46355	53.57	129	224	1.4	1.24	1.31	0.25	0.58	2.2	28.8	64.3	2.0
			SSK46363	55.46	236	414	2.45	1.93	2.47	0.87	2.04	21.0	49.3	28.3	0.7

Table 3

European Substage	Goniatite Biozone	W. European Marine Band	BGS Sample	Depth (m)	HI_{pd} (mg/g TOC_{pd})	HI_o (mg/g TOC_o)	TOC_{pd} (%)	TOC_{pdNGOC} (%)	TOC_o (%)	ΔTOC (TOC_o-TOC_{pdNGOC}) (%)	FSI	Type I	Type II	Type III	Type IV
Arnsbergian	E_2		SSK46364	234.80	82	438	3.01	2.41	3.84	1.43	1.75	22.46	56.88	11.00	0.33
			SSK46366	235.38	212	473	4.00	2.83	4.74	1.90	2.16	29.46	52.54	12.67	0.00
			SSK46369	235.98	127	486	4.46	3.53	6.02	2.49	1.44	21.96	70.37	4.00	0.00
			SSK51175	236.70	101	402	3.83	3.13	4.76	1.62	1.42	15.61	56.05	27.00	0.33
			SSK51178	237.59	153	487	3.07	2.25	3.83	1.59	2.85	36.29	43.05	17.33	0.00
			SSK51180	237.90	94	384	2.49	1.96	2.91	0.95	1.77	17.59	49.41	24.67	0.33
			SSK51182	238.46	213	458	4.48	3.23	5.29	2.06	2.16	28.61	50.73	12.33	0.00
			SSK51184	238.86	238	504	4.48	3.11	5.44	2.33	2.58	36.12	48.21	13.67	0.00
			SSK51186	239.40	150	460	2.10	1.44	2.36	0.92	2.48	31.52	45.48	15.67	0.33
			SSK51188	239.80	246	531	5.70	4.00	7.28	3.28	3.34	45.53	37.81	16.00	0.00
			SSK51190	240.39	179	478	3.23	2.31	3.90	1.58	3.14	37.49	38.51	19.67	0.00
			SSK51192	240.93	190	383	3.30	2.41	3.57	1.16	1.34	13.88	53.79	30.33	0.33
		E_{2b}?	SSK51194	241.39	218	425	4.70	3.43	5.37	1.94	1.51	18.77	56.56	24.33	0.00
			SSK51197	242.15	128	412	1.65	1.13	1.74	0.61	1.58	18.81	54.85	19.33	1.00
			SSK51200	242.80	207	406	4.74	3.54	5.40	1.86	1.46	16.91	55.09	26.00	0.00
			SSK51202	243.28	231	405	6.63	4.92	7.51	2.58	2.15	23.45	43.55	25.67	4.67
			SSK51204	243.67	208	568	8.55	6.46	12.49	6.03	3.63	53.22	35.11	9.00	0.00
			SSK51206	244.09	172	570	8.16	6.41	12.41	6.01	4.32	59.53	23.81	13.00	0.67
			SSK51208	244.51	203	593	7.94	5.99	12.07	6.08	4.19	61.85	26.82	6.67	1.00
			SSK51210	245.14	173	540	8.72	6.88	12.71	5.83	2.79	41.73	48.60	6.67	0.00
			SSK51212	245.50	198	563	7.50	5.67	10.87	5.20	2.84	44.48	49.52	5.33	0.33
			SSK51214	246.11	190	472	7.20	5.53	9.24	3.71	2.14	28.88	53.12	13.67	0.67
			SSK52580	246.20	175	503	6.79	5.27	9.21	3.93	2.58	35.96	48.04	13.67	0.67
			SSK52582	246.98	298	555	7.55	5.03	9.51	4.48	3.84	53.08	30.92	14.33	0.67
			SSK53128	247.37	286	607	6.43	4.25	8.78	4.53	4.47	64.80	24.20	10.33	0.00
			SSK53130	247.92	174	394	6.55	5.13	7.71	2.58	1.43	15.78	54.22	26.00	1.00
			SSK53132	248.49	280	579	7.18	4.85	9.55	4.70	4.71	63.53	19.14	13.67	0.33
Pendleian (?)	E_1?		SSK53135	249.22	286	597	9.29	6.38	12.93	6.55	4.36	63.29	23.71	12.67	0.00
			SSK53137	249.66	235	568	6.92	4.95	9.57	4.62	3.92	55.73	29.94	12.67	0.00
			SSK53139	250.08	245	411	5.90	4.22	6.49	2.27	1.16	14.31	61.69	21.67	0.33
			SSK53141	250.80	243	437	5.97	4.25	6.76	2.51	2.27	27.19	45.48	23.33	1.00
			SSK53144	251.29	198	352	4.57	3.43	4.90	1.46	1.29	12.61	48.39	32.33	1.33
			SSK53146	251.89	203	360	4.98	3.70	5.33	1.63	1.23	11.83	50.50	36.00	0.67

Table 4

Formation	(Sub)System	HI_o (mg/g TOC_o)	TOC_o (%)
US Shales (Jarvie, 2012)			
Barnett	Mississippian	434	6.27
Fayetteville	Mississippian	404	6.32
Woodford	Devonian	503	8.95
Bossier	Upper Jurassic	419	2.75
Haynesville	Upper Jurassic	722	5.05
Marcellus	Devonian	507	7.83
Muskwa	Devonian	532	3.62
Montney	Triassic	354	3.27
Utica	Ordovician	379	2.23
Eagle Ford	Upper Cretaceous	411	4.63
United Kingdom (this study)			
Widmerpool Gulf (E_{2a3}–E_{2b1})	Mississippian	465	3.2
Widmerpool Gulf (E_{2a} below E_{2a3})	Mississippian	396	1
Edale Gulf (E_{2b} (?) and above)	Mississippian	448	4.4
Edale Gulf (E_{2a}–E_1)	Mississippian	504	9.3

Table 5

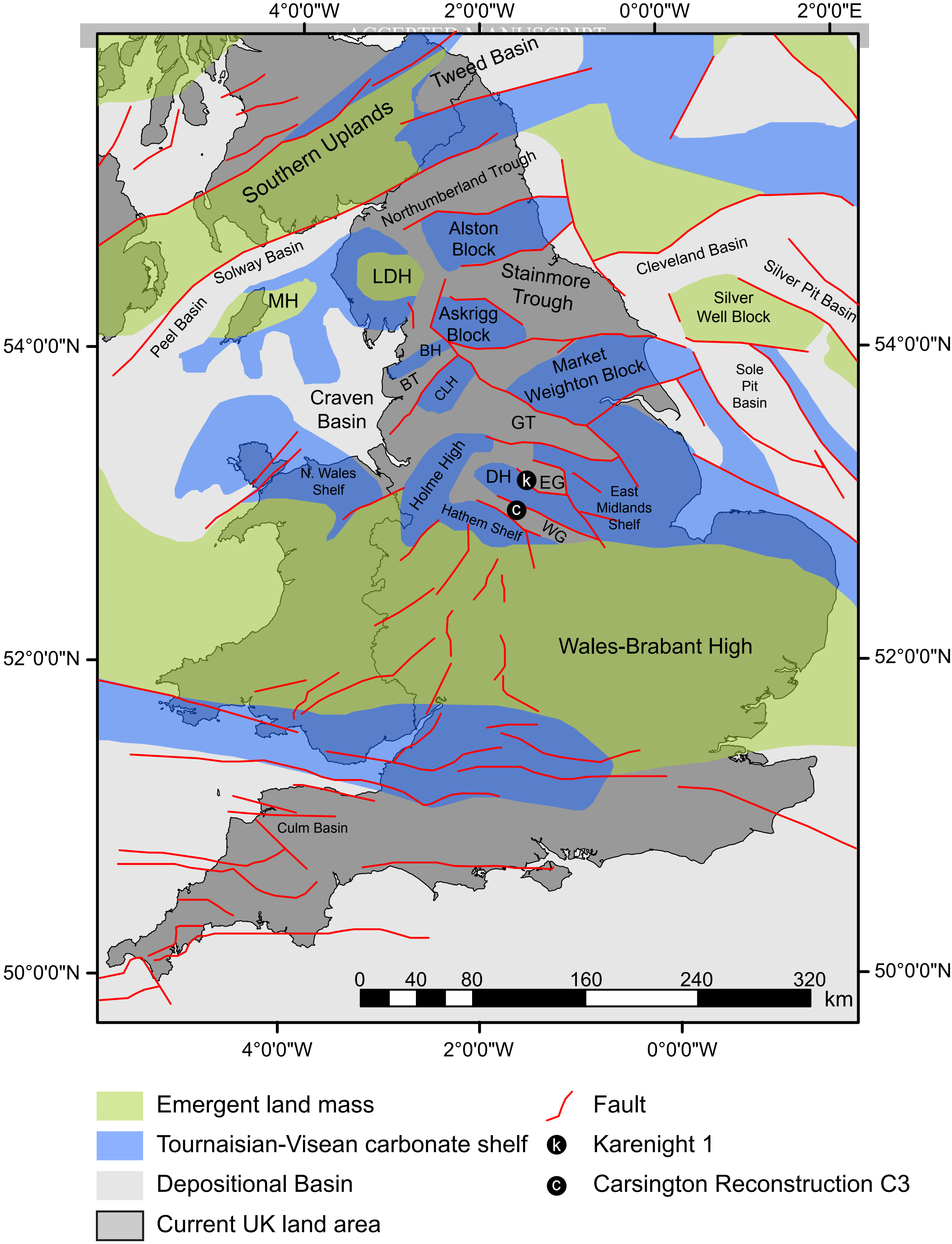
4°0'0"W
2°0'0"W
0°0'0"W
2°0'0"E
Tweed Basin
Southern Uplands
Northumberland Trough
Alston Block
Solway Basin
LDH
MH
Peel Basin
Stainmore Trough
Askrigg Block
Cleveland Basin
Silver Pit Basin
Silver Well Block
BH
BT
CLH
Market Weighton Block
Sole Pit Basin
Craven Basin
GT
N. Wales Shelf
Holme High
DH
EG
East Midlands Shelf
Hathem Shelf
WG
Wales-Brabant High
Culm Basin
54°0'0"N
52°0'0"N
50°0'0"N
0
40
80
160
240
320
km
Emergent land mass
Tournaisian-Visean carbonate shelf
Depositional Basin
Current UK land area
Fault
Karenight 1
Carsington Reconstruction C3

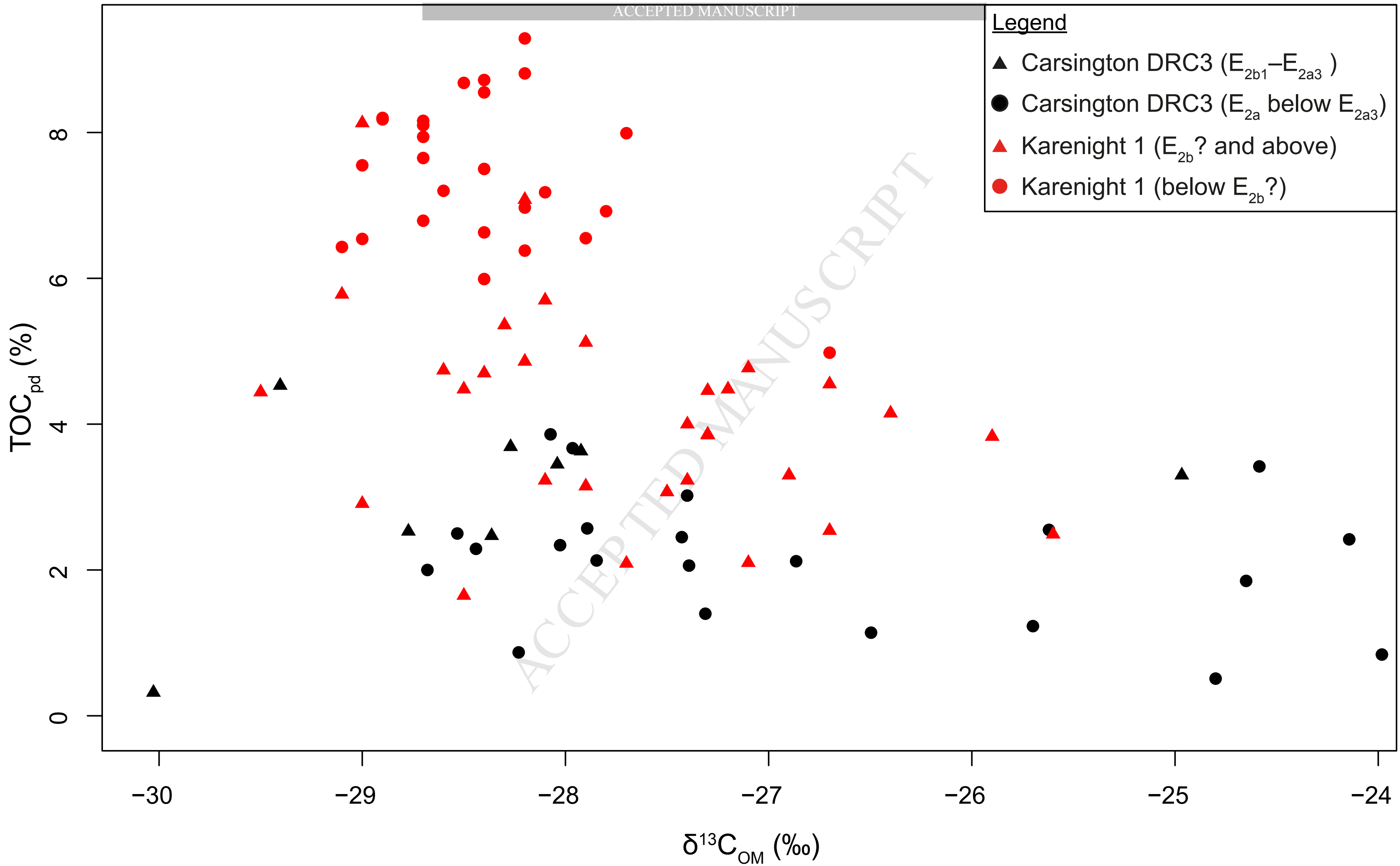
Legend
Carsington DRC3 (E2b1–E2a3)
Carsington DRC3 (E2a below E2a3)
Karenight 1 (E2b? and above)
Karenight 1 (below E2b?)
TOCpd (%)
0
2
4
6
8
−30
−29
−28
−27
−26
−25
−24
δ13COM (‰)

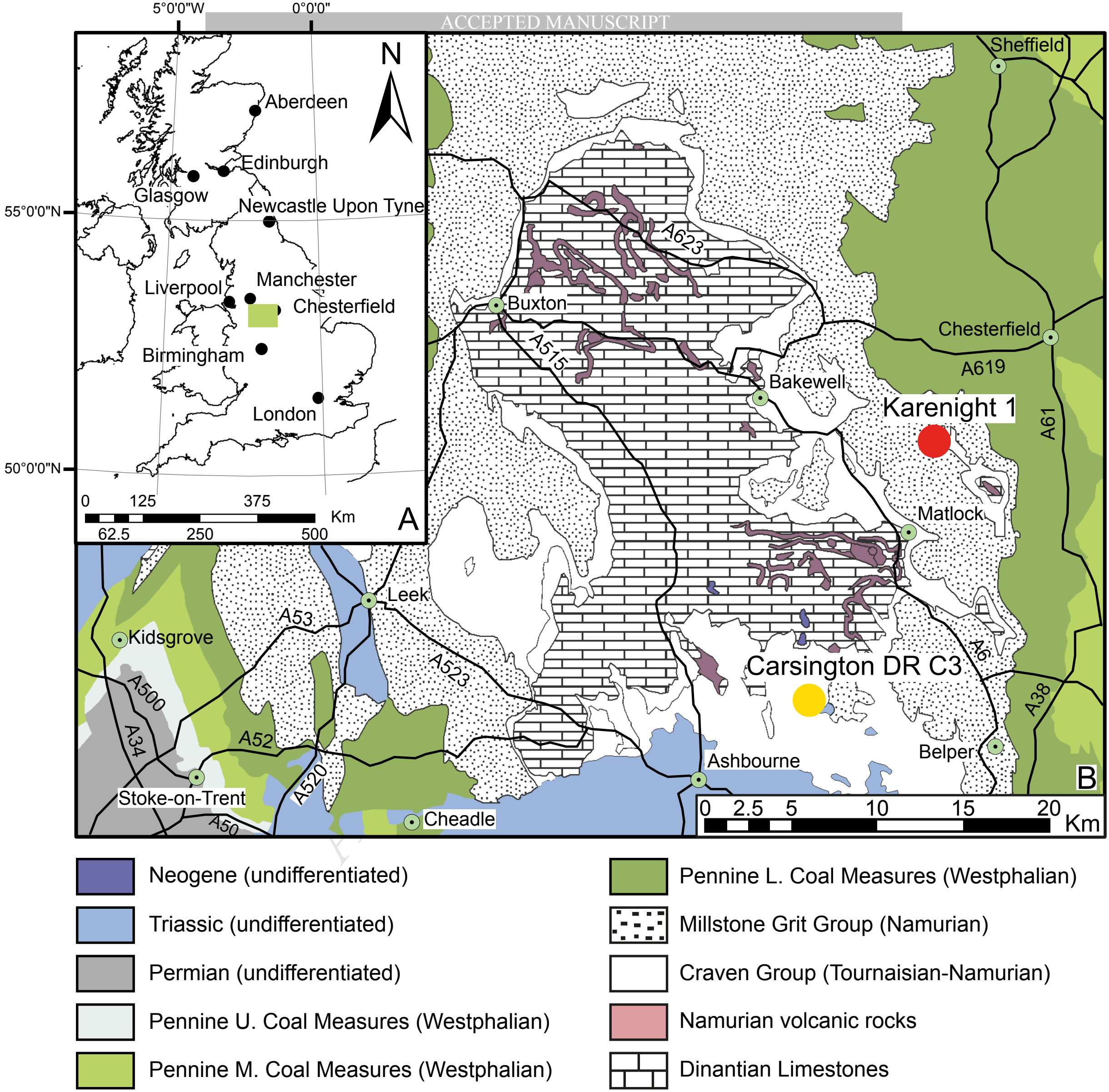
5°0'0"W
0°0'0"
55°0'0"N
50°0'0"N
N
Aberdeen
Edinburgh
Glasgow
Newcastle Upon Tyne
Manchester
Liverpool
Chesterfield
Birmingham
London
0
125
375
Km
62.5
250
500
A
Sheffield
Buxton
A623
A515
Chesterfield
A619
Bakewell
Karenight 1
A61
Matlock
Leek
A53
Kidsgrove
A523
A500
A34
A52
A520
Stoke-on-Trent
A50
Cheadle
Ashbourne
Carsington DR C3
A6
A38
Belper
B
0
2.5
5
10
15
20
Km
Neogene (undifferentiated)
Triassic (undifferentiated)
Permian (undifferentiated)
Pennine U. Coal Measures (Westphalian)
Pennine M. Coal Measures (Westphalian)
Pennine L. Coal Measures (Westphalian)
Millstone Grit Group (Namurian)
Craven Group (Tournaisian-Namurian)
Namurian volcanic rocks
Dinantian Limestones

Global Chrono-stratigraphy
Regional Chrono-stratigraphy
United States
United Kingdom Basins
Age (Ma)
Period
Epoch
Stage
N. American Stage
Eur. Stages (obs.)
W. European Stage
U.K. Substage
Fort Worth Basin
Bowland Basin
Derbyshire High - Edale Gulf
Widmerpool Gulf
Davydov et al. (2012)
Holliday and Molyneux (2007)
Pollastro et al. (2003; 2007)
Waters et al. (2007)
299
307
315
323
331
339
347
359
Carboniferous
Pennsylvanian
Mississippian
Upper
Middle
Lower
Gzhelian
Kasimo.
Moscovian
Bashkirian
Serpukhovian
Visean
Tournaisian
Virgilian
Missour.
Desmoinesian
Atokan
Morrowan
Chesterian
Meramecian
Osagean
Kinderhookian
Rotlieg.
Silesian
Dinantian
Autunian
Stephanian
Westphalian
Namurian
Visean
Tournaisian
Kuzel
Steph. C
Steph. B
Steph. A
Cantabrian
Asturian
Bolsovian
Duckmant.
Langs.
Yead.
Mars.
Kinder. Alportian
Chokie.
Arnsbergian
Pendl.
Brigant.
Asbian
Holkerian
Arund.
Chad.
Courceyan
Cisco
Thrifty Group
Graham Group
Canyon
Caddo Cr. Gr.
Brad Gr.
Graford Gr.
Whitt Gr.
Strawn
Lone Camp Gr.
Millsap Lake Gr.
Kickapoo Gr.
Caddo II/III
Sm.
Pregnant
Smithwick
Atoka Fm.
Smith-wick
Big Saline
Morrow Fm.
Marble Falls Fm.
Comyn Formation
Upper Barnett Shale
Forestburg Limestone
Lower Barnett Shale
Chappel Limestone Formation
Pennine Coal Measures
Halesowen Formation
Etruria
Pennine Upper Measures Fm.
Pennine Middle Measures Fm.
Hebden
Millstone Grit Group
Rossendale Fm.
Marsden Formation
Hebden
Samles
Fm.
Silsden Formation
Pendle-ton
Bowland Shale Formation
Craven Group
Pendleside
Hodderense Fm.
Hodder Mudstone Formation
Clitheroe
Bowland High Group
Chatburn Limestone Fm.
Craven Group
Morridge Fm.
Bowland Shale Gr.
Widmer-pool Fm.
Ecton Limestone Fm.
Peak Limestone Group
Milldale Limestone Formation
Rue Hill Dolomite Fm.
Redhouse Sandstone Fm.
Etruria Formation
Pennine Upper Measures Fm.
Pennine Middle Measures Fm.
PLCM
Ross. Fm.
Mars.
Morridge Fm.
Bowland Shale Formation
Widmerpool Formation
Lockington Limestone
Long Eaton Formation
Hathern Anhydrite Formation

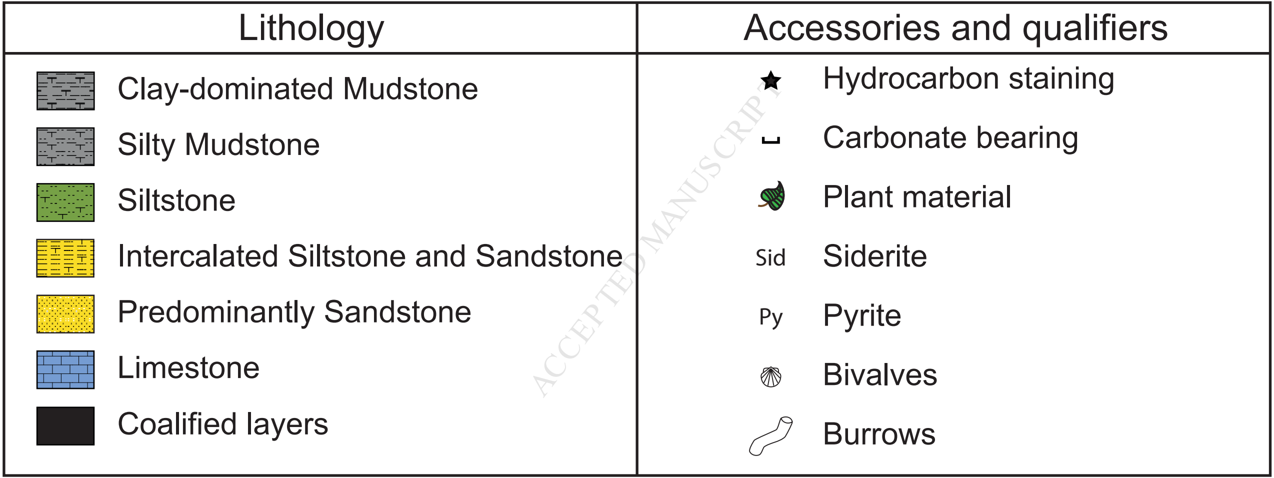
Lithology
Clay-dominated Mudstone
Silty Mudstone
Siltstone
Intercalated Siltstone and Sandstone
Predominantly Sandstone
Limestone
Coalified layers
Accessories and qualifiers
Hydrocarbon staining
Carbonate bearing
Plant material
Sid
Siderite
Py
Pyrite
Bivalves
Burrows

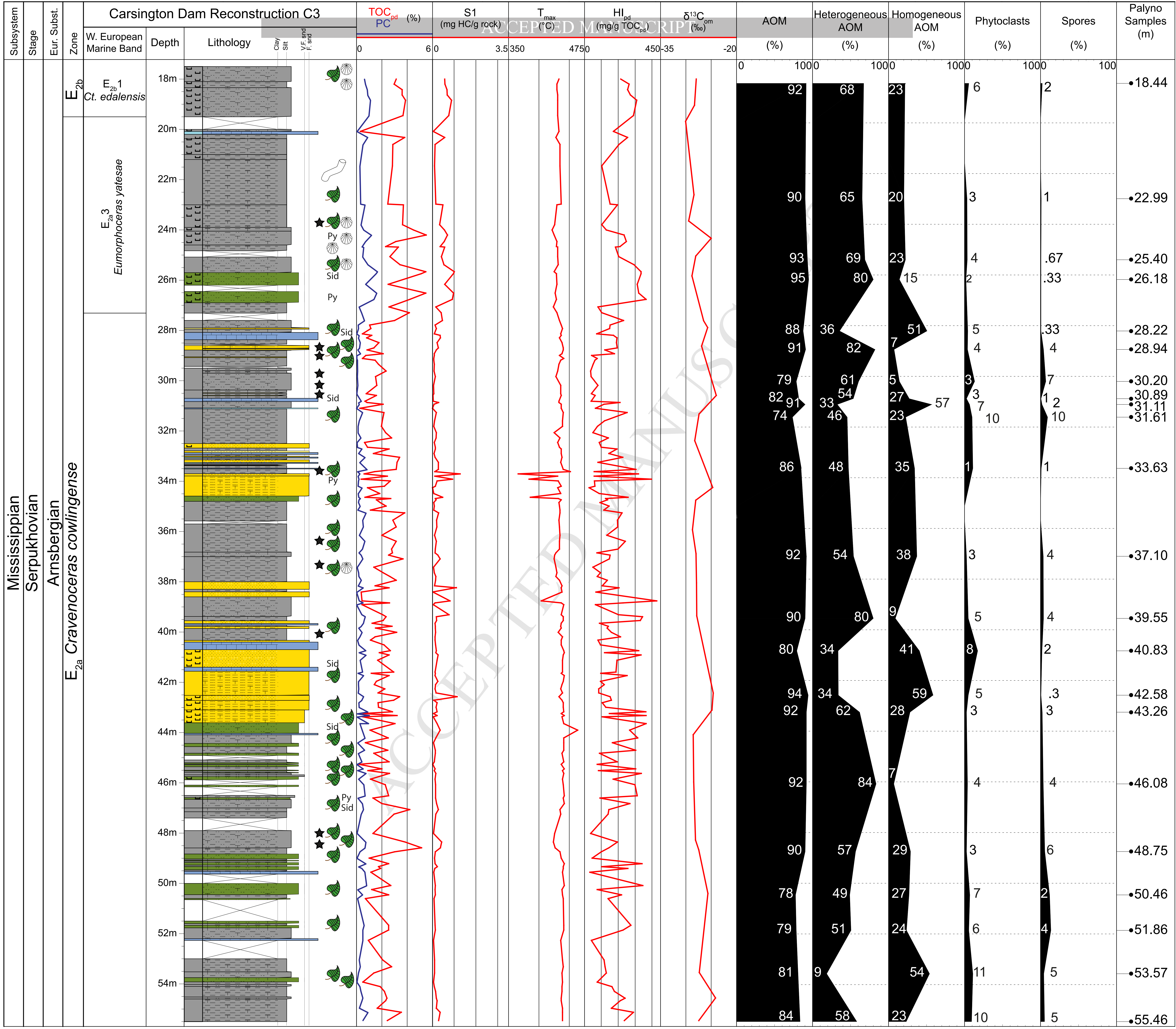

Carsington Dam Reconstruction C3
Subsystem
Stage
Eur. Subst.
Zone
W. European Marine Band
Depth
Lithology
TOC pd PC (%)
S1 (mg HC/g rock)
T max (°C)
HI pd (mg/g TOC pd)
δ13C om (‰)
AOM (%)
Heterogeneous AOM (%)
Homogeneous AOM (%)
Phytoclasts (%)
Spores (%)
Palyno Samples (m)
Mississippian
Serpukhovian
Arnsbergian
E2a Cravenoceras cowlingense
E2b
E2b1 Ct. edalensis
E2a3 Eumorphoceras yatesae
Py
Sid
ACCEPTED MANUSCRIPT

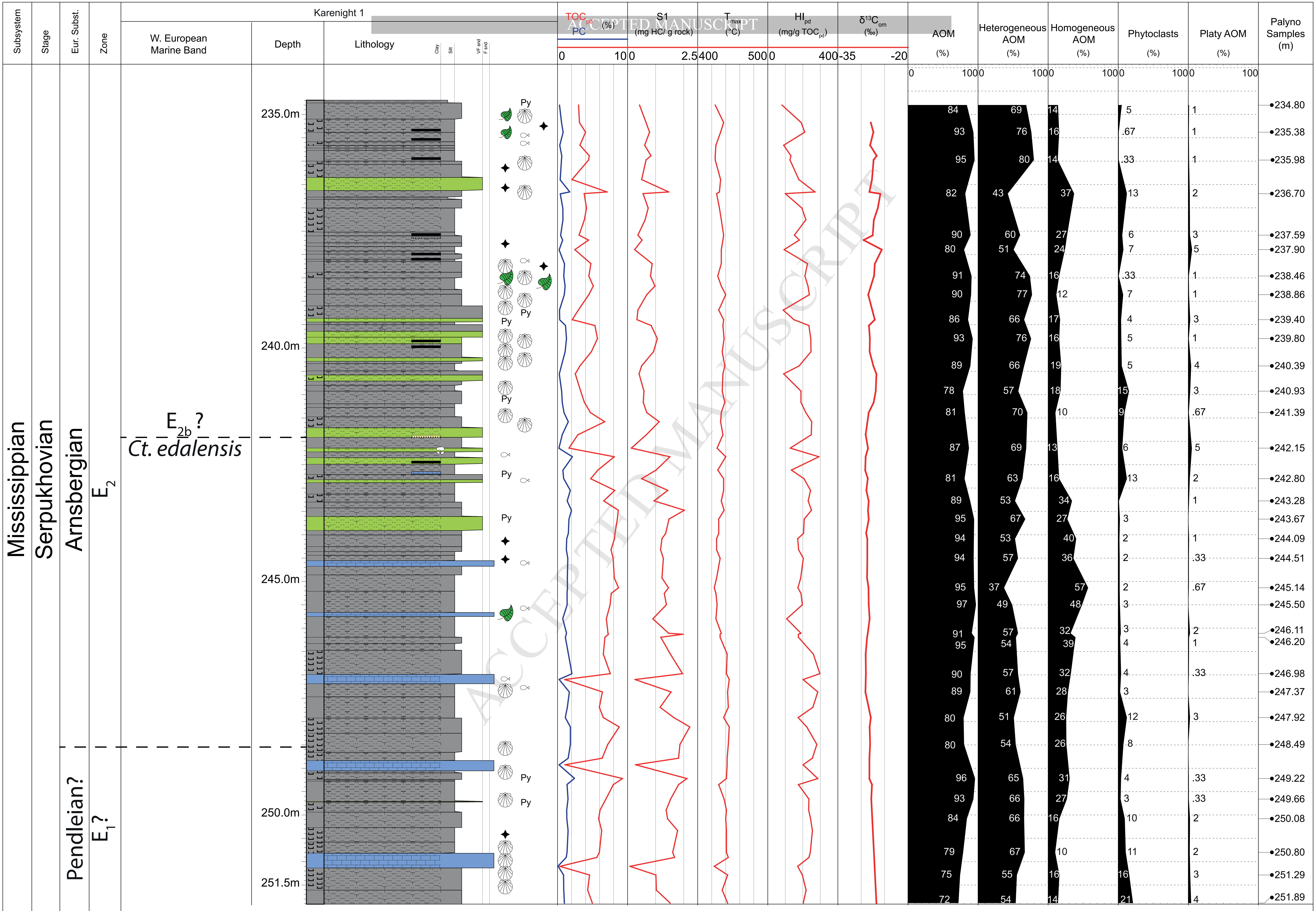
Subsystem
Stage
Eur. Subst.
Zone
Karenight 1
W. European Marine Band
Depth
Lithology
Clay
Silt
VF snd
F snd
TOCpd PC (%)
0 10
S1 (mg HC/ g rock)
0 2.5
Tmax (°C)
400 500
HIpd (mg/g TOCpd)
0 400
δ13Com (‰)
-35 -20
AOM (%)
Heterogeneous AOM (%)
Homogeneous AOM (%)
Phytoclasts (%)
Platy AOM (%)
0 100
Palyno Samples (m)
Mississippian
Serpukhovian
Arnsbergian
E2
Pendleian?
E1?
E2b ?
Ct. edalensis
235.0m
240.0m
245.0m
250.0m
251.5m
Py
234.80
235.38
235.98
236.70
237.59
237.90
238.46
238.86
239.40
239.80
240.39
240.93
241.39
242.15
242.80
243.28
243.67
244.09
244.51
245.14
245.50
246.11
246.20
246.98
247.37
247.92
248.49
249.22
249.66
250.08
250.80
251.29
251.89

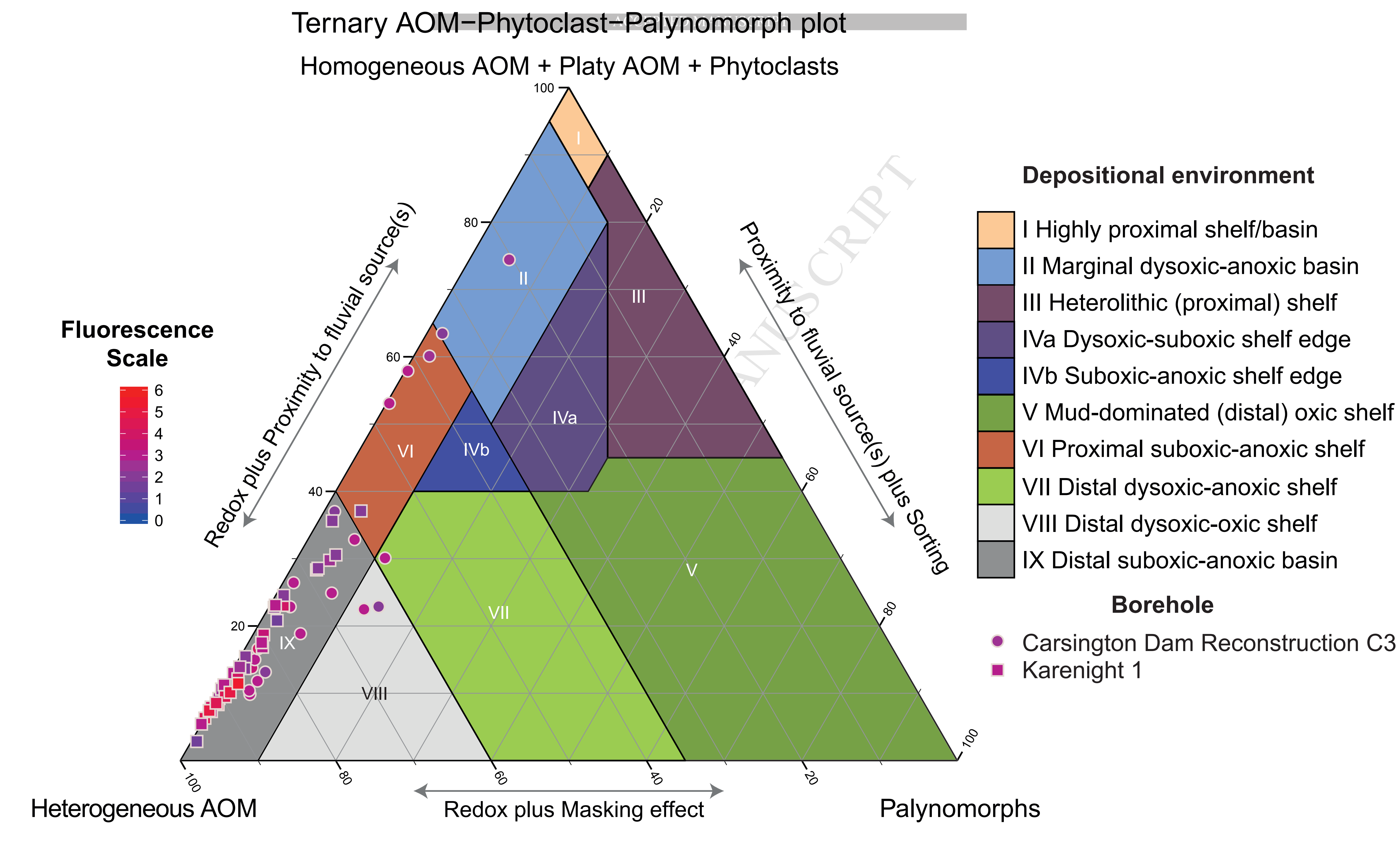

Ternary AOM−Phytoclast−Palynomorph plot
Homogeneous AOM + Platy AOM + Phytoclasts
Heterogeneous AOM
Palynomorphs
Redox plus Proximity to fluvial source(s)
Proximity to fluvial source(s) plus Sorting
Redox plus Masking effect
100
80
60
40
20
I
II
III
IVa
IVb
V
VI
VII
VIII
IX
Fluorescence Scale
6
5
4
3
2
1
0
Depositional environment
I Highly proximal shelf/basin
II Marginal dysoxic-anoxic basin
III Heterolithic (proximal) shelf
IVa Dysoxic-suboxic shelf edge
IVb Suboxic-anoxic shelf edge
V Mud-dominated (distal) oxic shelf
VI Proximal suboxic-anoxic shelf
VII Distal dysoxic-anoxic shelf
VIII Distal dysoxic-oxic shelf
IX Distal suboxic-anoxic basin
Borehole
Carsington Dam Reconstruction C3
Karenight 1

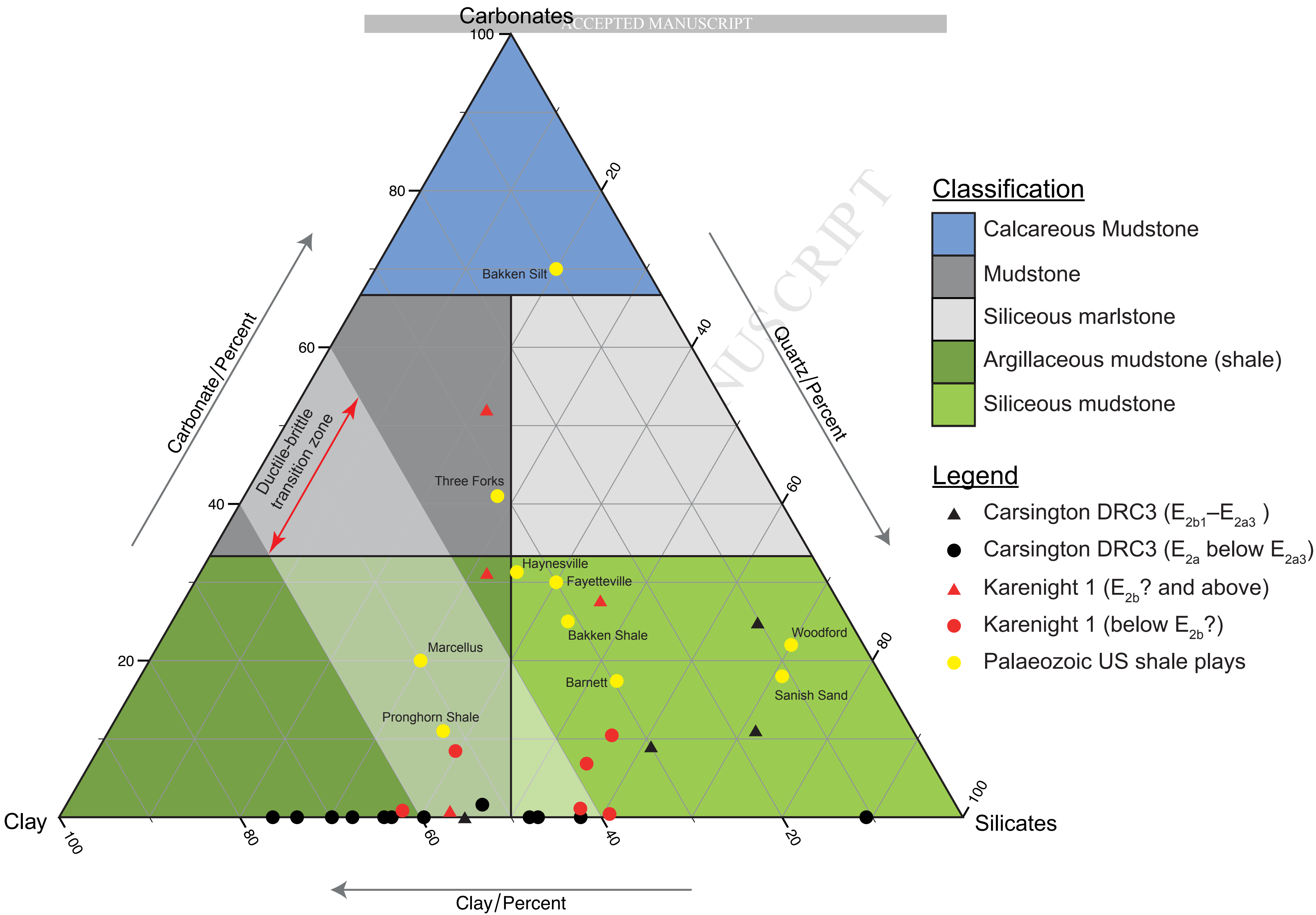

Carbonates
Clay
Silicates
Carbonate/Percent
Quartz/Percent
Clay/Percent
Ductile-brittle transition zone
100
80
60
40
20
Bakken Silt
Three Forks
Haynesville
Fayetteville
Bakken Shale
Marcellus
Woodford
Barnett
Sanish Sand
Pronghorn Shale
Classification
Calcareous Mudstone
Mudstone
Siliceous marlstone
Argillaceous mudstone (shale)
Siliceous mudstone
Legend
Carsington DRC3 (E_{2b1}–E_{2a3})
Carsington DRC3 (E_{2a} below E_{2a3})
Karenight 1 (E_{2b}? and above)
Karenight 1 (below E_{2b}?)
Palaeozoic US shale plays

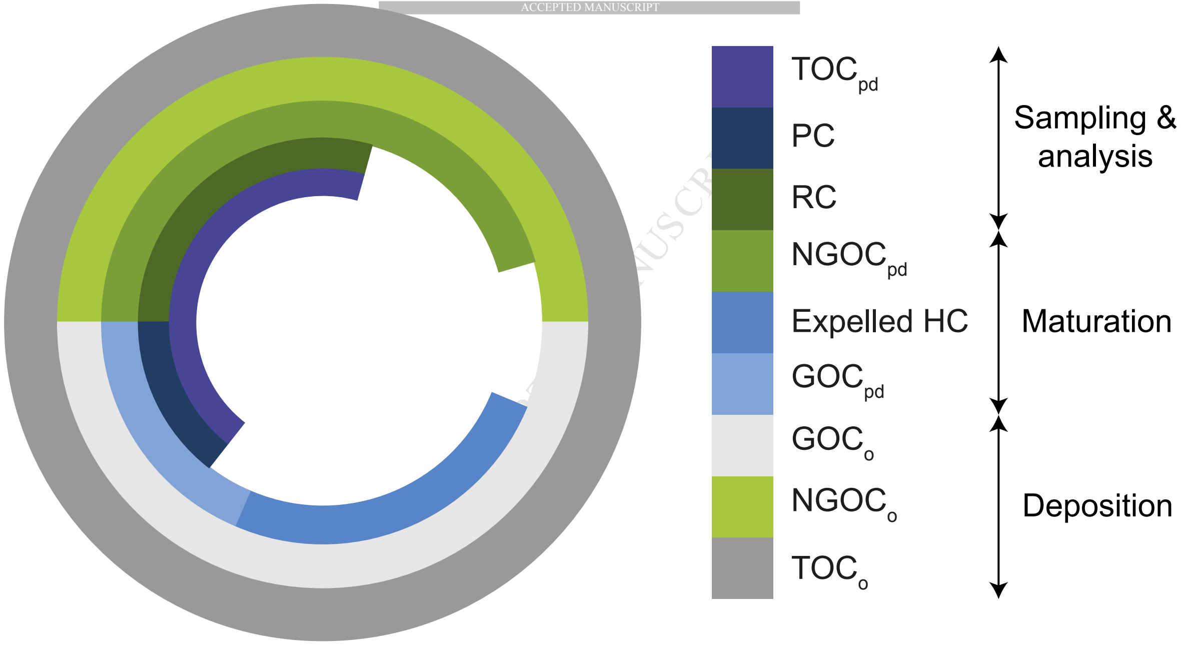

TOC$_{pd}$
PC
RC
NGOC$_{pd}$
Expelled HC
GOC$_{pd}$
GOC$_{o}$
NGOC$_{o}$
TOC$_{o}$
Sampling & analysis
Maturation
Deposition

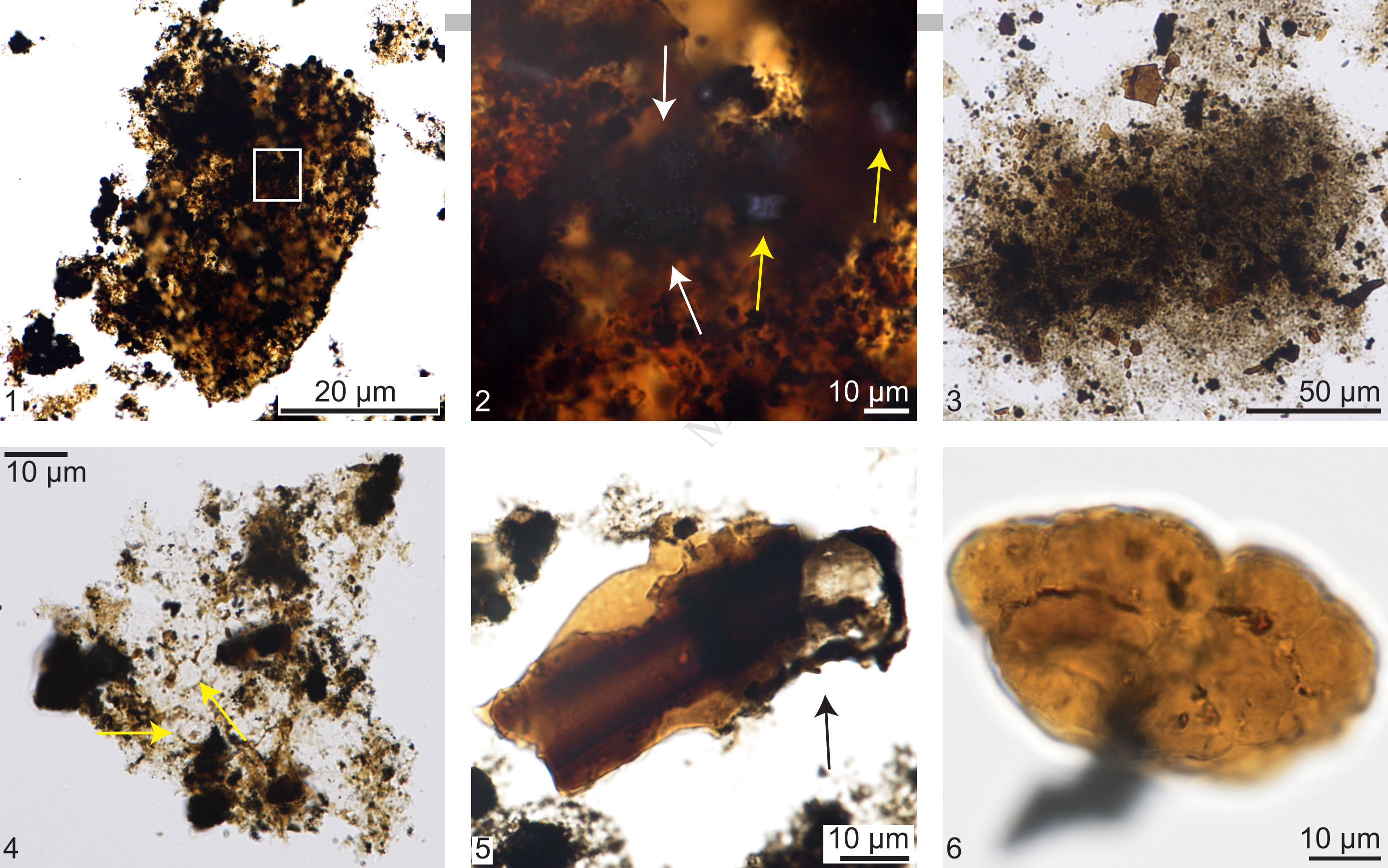
1
20 μm
2
10 μm
3
50 μm
10 μm
4
5
10 μm
6
10 μm

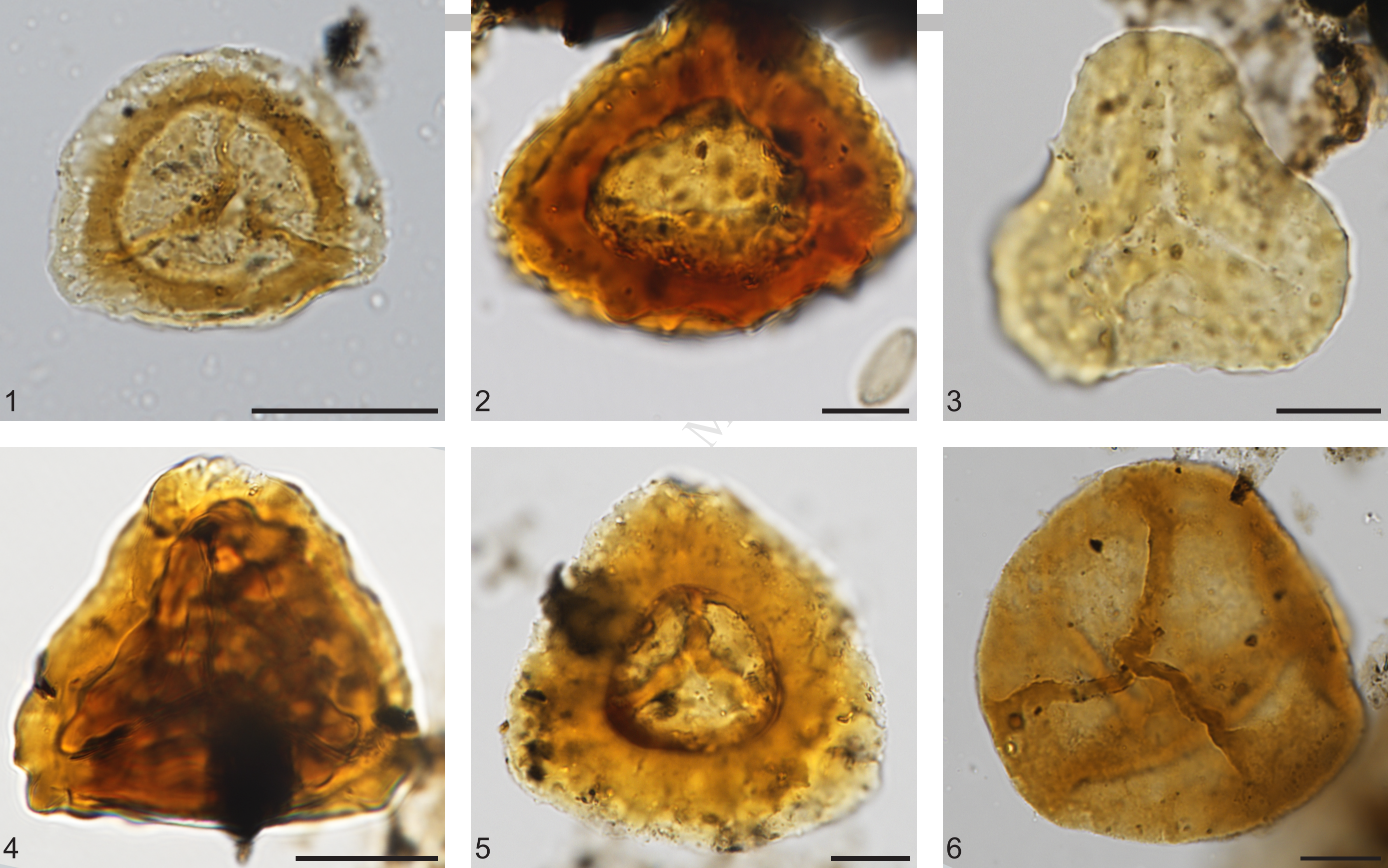
1
2
3
4
5
6

Highlights

- Palynofacies analysis and Rock Eval™ establish HI_o and TOC_o for the Morridge Fm.
- TOC_o for Namurian deposits in the Widmerpool Gulf fluctuates between 3 and 13%
- TOC_o for Namurian deposits in the Edale Gulf fluctuates between 4 and 14%
- T_{max} shows the Morridge Formation is immature for gas in the Southern Pennine Basin